

1 **CvkR, a novel MerR-type transcriptional regulator, is a repressor of**  
2 **class 2 type V-K CRISPR-associated transposase systems**

3

4 Marcus Ziemann<sup>1\*</sup>, Viktoria Reimann<sup>1\*</sup>, Yajing Liang<sup>2,3,4\*</sup>, Yue Shi<sup>2,3,4</sup>, Yuman Xie<sup>2,5</sup>,  
5 Hui Li<sup>2,5</sup>, Tao Zhu<sup>2,3,4,5,#</sup>, Xuefeng Lu<sup>2,3,4,5,6,#</sup>, Wolfgang R. Hess<sup>1,#</sup>

6

7 <sup>1</sup>University of Freiburg, Faculty of Biology, Institute of Biology III, Genetics and  
8 Experimental Bioinformatics, Schänzlestr. 1, D-79104, Germany;

9 <sup>2</sup>Qingdao Institute of Bioenergy and Bioprocess Technology (QIBEBT), Chinese  
10 Academy of Sciences, No.189 Songling Road, Qingdao 266101, China;

11 <sup>3</sup>Shandong Energy Institute, Qingdao 266101, China;

12 <sup>4</sup>Qingdao New Energy Shandong Laboratory, Qingdao 266101, China;

13 <sup>5</sup>University of Chinese Academy of Sciences, Beijing 100049, China;

14 <sup>6</sup>Laboratory for Marine Biology and Biotechnology, Qingdao National Laboratory for  
15 Marine Science and Technology, Qingdao 266237, China

16

17 **#Authors for correspondence:**

18 Wolfgang R. Hess: Phone: +49-761-203-2796; FAX: +49-761-203-2745; Email:  
19 [wolfgang.hess@biologie.uni-freiburg.de](mailto:wolfgang.hess@biologie.uni-freiburg.de);

20 Xuefeng Lu: Phone: +86-532-80662712; FAX: +86-532-80662778; Email:  
21 [lvxf@qibebt.ac.cn](mailto:lvxf@qibebt.ac.cn);

22 Tao Zhu: Phone: +86-532-80662711; FAX: +86-532-80662778; Email:  
23 [zhutao@qibebt.ac.cn](mailto:zhutao@qibebt.ac.cn);

24

25 \*shared first authorships

26

27

28 **Running head:** Transcriptional regulation of CAST systems

29 **Keywords:** CRISPR, CRISPR-associated transposons, cyanobacteria, transcriptional  
30 regulator

31 **Abstract**

32 CRISPR-associated transposons (CASTs) exist in different groups of bacteria,  
33 including certain cyanobacteria, which contain type V-K CAST systems. These  
34 systems contain genes encoding Tn7-like transposase subunits and a divergent  
35 number of cargo genes. How the activity of these systems is controlled *in situ* has  
36 remained largely unknown but possibly regulatory genes within these elements are  
37 prime candidates. Deletion of the respective regulator gene *alr3614* in the  
38 cyanobacterium *Anabaena (Nostoc) sp. PCC 7120* led to the overexpression of  
39 CRISPR tracrRNA, precursor crRNAs and mRNAs encoding the Cas12k effector  
40 protein (*all3613*) and Tn7-like transposase subunits. Upon complementation, these  
41 same genes were repressed again. DNase I footprinting and electrophoretic mobility  
42 shift assays verified the direct interaction between Alr3614 and the promoter of *cas12k*  
43 and identified a widely conserved binding motif. Structural analysis of Alr3614 at 1.5 Å  
44 resolution revealed that it belongs to the MerR-type transcription factor family but with  
45 distinct dimerization and effector-binding domains. This protein assembles into a  
46 homodimer interacting with DNA through its N-terminal winged helix-turn-helix (wHTH)  
47 domain and binds an effector molecule through a C-terminal  $\alpha$ -helical domain lacking  
48 a conserved cysteine. These results identify Alr3614 as a transcriptional repressor of  
49 the CAST system in *Anabaena sp. PCC 7120*. We suggest naming this family of  
50 repressors CvkR for Cas V-K repressors, which are at the core of a widely conserved  
51 regulatory mechanism that controls type V-K CAST systems.

52

## 53 Introduction

54 Native Clustered Regularly Interspaced Short Palindromic Repeats (CRISPRs) and  
55 CRISPR-associated (Cas) proteins are well characterized for their function as RNA-  
56 based adaptive and inheritable immune systems found in many bacteria and archaea<sup>1-</sup>  
57 <sup>6</sup>. Multiple genetic approaches developed from these native CRISPR-Cas systems  
58 have become popular for the manipulation of gene expression and genome editing<sup>7-9</sup>.  
59 CRISPR-Cas systems are extremely diverse and are classified into 2 classes, 6 types  
60 and 33 subtypes<sup>10</sup>. Recently, a remarkable group of derivatives has been discovered  
61 that constitute hybrids of Tn7-like transposons and CRISPR systems encoding Cas12k  
62 effectors with naturally inactivated nuclease domains<sup>11</sup> or encoding Cascade  
63 complexes lacking the Cas3 nuclease component<sup>12,13</sup>. The respective transposon-  
64 associated CRISPR systems include class 1 type I-F, I-B, and class 2 type V-K  
65 systems<sup>13</sup>. These systems, called CRISPR-associated transposons (CASTs), are  
66 capable of catalyzing the transposition of mobile genetic elements guided by crRNAs,  
67 while the type I-B associated systems use a dedicated TniQ/TnsD protein-based  
68 homing mechanism<sup>13</sup>.

69 The system characterized from *Vibrio cholerae* consists of genes encoding the subtype  
70 I-F CRISPR-Cas proteins Cas6, Cas7, and Cas8 and genes encoding the transposon  
71 proteins TnsA, TnsB, TnsC and TniQ<sup>12</sup>. A single instance of a class 1 type I-B and of  
72 several class 2 type V-K CAST systems have been reported in several different  
73 cyanobacteria, which constitute a rich natural resource for these systems<sup>11,13,14</sup>.

74 The V-K CAST systems, first characterized in *Scytonema hofmanni*<sup>11</sup>, contain genes  
75 encoding the effector complex subunit Cas12k and the Tn7-like transposase subunits  
76 TnsB, TnsC and TniQ, while *tnsA* is lacking. Targeting transposition by these CAST  
77 systems depends on the DNA-crRNA interaction facilitated by the effector protein  
78 Cas12k<sup>11</sup>. The TnsC transposon then forms helical polymers around the DNA

79 supported by ATP binding<sup>15</sup>. The growth in the 5' to 3' direction is stopped by TniQ  
80 binding at the filament end concomitantly connecting the TnsC filament with Cas12k.  
81 On the other filament end, the Mu-like transposase TnsB then starts to integrate the  
82 transposon<sup>15</sup>. In addition to the genes encoding transposase and effector proteins, all  
83 of these systems contain various numbers of cargo genes. Novel genetic approaches  
84 have been developed from the different Tn7-CRISPR–Cas hybrid systems<sup>16–18</sup>,  
85 underlining that the better characterization of such systems is of both fundamental and  
86 applied interest.

87 While the paradigm is that native CRISPR-Cas systems primarily protect genome  
88 integrity against mobile genetic elements, the CAST systems seem to violate this  
89 paradigm since they constitute transposable elements by definition. Thus, the tight  
90 regulation of these systems can be expected. Indeed, CAST systems have also been  
91 reported to contain a gene encoding a putative MerR-type transcriptional regulator<sup>14</sup>,  
92 but this association has not been systematically investigated, nor has its function been  
93 addressed experimentally thus far.

94 We have studied the CRISPR-Cas systems in *Anabaena (Nostoc) sp.* PCC 7120 (from  
95 here: *Anabaena* 7120), a multicellular nitrogen-fixing model cyanobacterium with a  
96 CRISPR-rich chromosome of eleven CRISPR-like repeat-spacer cassettes. All of them  
97 are transcribed<sup>14</sup>, and based on the specificities of the cognate Cas6 maturation  
98 endonucleases, five of these arrays were assigned to a type III-D and another five to  
99 a type I-D CRISPR-Cas system<sup>19</sup>, while the remaining array (CR\_9) belongs to a  
100 separate CRISPR type with all the hallmarks of a CAST system<sup>14,19</sup>.

101 Here, we first scrutinized the association between putative transcriptional regulators  
102 and cyanobacterial CAST systems and found these to belong to four different classes.  
103 We then investigated the Alr3614 transcriptional regulator belonging to the *Anabaena*  
104 7120 CRISPR-associated transposase (AnCAST) system. We found that both the

105 *cas12k* gene *all3613* and the *merR*-like gene *alr3614* are translated from leaderless  
106 mRNAs. In the deletion mutant  $\Delta alr3614$ , we observed overexpression of the AnCAST  
107 core module, while repression was restored if Alr3614 was expressed from a  
108 complementing plasmid vector. Hence, Alr3614 functions as a repressor of AnCAST.  
109 The crystal structure analysis at 1.5 Å resolution was consistent with the assignment  
110 of Alr3614 to the MerR-type family of transcription factors but also revealed specific  
111 features within the dimerization and effector-binding domains. It assembles into a  
112 homodimer interacting with DNA through its N-terminal winged helix-turn-helix (wHTH)  
113 domain and binds effector molecule(s) through its C-terminal domain with a standard  
114  $\alpha$ -helix and lacking the cysteine otherwise widely conserved in this type of regulator.  
115 We suggest naming Alr3614 and its functional homologs Cas V-K repressor (CvkR)  
116 encoded by the gene *cvkR*.  
117 While almost all CAST systems contain a regulatory gene, phylogenetic analyses  
118 suggested that different repressor types can be encoded at the corresponding location,  
119 belonging to the Arc repressor superfamily (CopG- and Omega-like repressors) and  
120 the MerR family, or appearing as a different class of putative HTH domain-containing  
121 proteins. Our results illuminate the role of CvkR regulators in controlling the activity of  
122 CAST systems.

123

## 124 **Results**

### 125 ***Architecture of cyanobacterial CAST systems***

126 Starting from the known CAST components, we searched for conserved genes and  
127 genetic elements in their vicinity. These elements included the left and right ends (LE  
128 and RE) of the transposon, the neighboring tRNA, CRISPR arrays and tracrRNA, the  
129 transposase genes (*tniQ*, *tnsC* and *tnsB*), and genes in reverse orientation next to the  
130 start codon of *cas12k* predicted to encode small DNA-binding proteins. We identified

131 118 CAST systems with a clear *cas12k* gene in 88 different strains. The majority of  
132 these were found in the Nostocales (60%), Chroococcales (15%), and  
133 Pseudanabaenales (11%), complemented by a small number of CAST systems in the  
134 Oscillatoriales, Pleurocapsales, Spirulinales and Synechococcales cyanobacteria  
135 (**Table S1**). Three additional CAST systems were found in unclassified filamentous  
136 cyanobacteria (CCT1, CCP 2 and 4). From this analysis, we could delineate the  
137 general structure of this type of CAST system (**Fig. 1**) consistent with previous  
138 analyses and extend them<sup>10,11,14</sup>.

139 The LE usually lies downstream of a tRNA gene oriented toward the transposon. The  
140 CRISPR array always follows in a short distance and in reverse orientation with regard  
141 to the tRNA gene. The majority of CRISPR repeats are 37 nt long with high  
142 conservation at the 3' end. There is also a sequence-conserved promoter upstream of  
143 the *tracrRNA*, which is followed or, in some cases, even overlapped by the CRISPR-  
144 Cas effector gene *cas12k*, transcribed in the same direction.

145 Next to the LE element, inside the transposon lies a truncated, single repeat  
146 downstream but usually clearly separated from the CRISPR array. Directly  
147 downstream of this repeat, a truncated spacer sequence of usually 17 nt can be  
148 identified that corresponds to a protospacer sequence just outside of the transposon  
149 next to the LE, usually within the tRNA gene<sup>13</sup>. The truncated single repeat-spacer  
150 sequences, read toward the LE, show a conserved upstream GTN-PAM, consistent  
151 with the predicted Cas12k PAM<sup>11</sup>. The distance from this PAM to the LE varies from  
152 46 to 82 nt, with one exception of 147 nt. Because of its conserved position at this site  
153 and experimental evidence of CAST integration via protospacer recognition<sup>13</sup>, this  
154 motif is likely necessary for the insertion of CAST. We therefore suggest the terms  
155 anchor protospacer and anchor spacer for these sequences.

156 Looking from the other side of the transposon, the first genes next to the RE are the  
157 three genes encoding transposase subunits TnsB, TnsC, and TniQ, always in this  
158 order, facing away from the RE. The majority of cargo genes, located between *cas12k*  
159 and *tniQ*, are significantly more divergent. There is, however, one exception, a gene  
160 predicted to encode a small DNA-binding protein next to the start codon of *cas12k* in  
161 reverse orientation.

162

163 ***MerR-type, Arc-type and HTH domain-containing transcriptional regulators are***  
164 ***associated with the CAST systems of cyanobacteria***

165 The genes encoding potential CvkRs were identified by their position and orientation  
166 with regard to the *cas12k* gene. We analyzed the first gene located upstream of *cas12k*  
167 in reverse orientation, assigned it to prominent gene families and then performed  
168 similarity searches against NCBI's non-redundant protein database. In total, we  
169 identified 94 CAST systems with genes encoding a putative regulator in a conserved  
170 position and orientation with regard to the *cas12k* gene. The *cvkR* genes occur once  
171 per CAST system; however, in some instances, degenerated *cvkR* duplicate genes  
172 exist immediately after the functional genes. Additionally, we found CAST systems with  
173 additional candidate genes but further away from *cas12k*, but none of those instances  
174 was considered further to avoid potentially misleading information.

175 The small DNA-binding proteins encoded by the CAST-associated regulatory genes  
176 contain either a helix-turn-helix (HTH) domain or a ribbon-helix-helix domain (RHH) for  
177 interaction with DNA. The bioinformatic analysis classified them as members of the  
178 MerR family (53 CvkRs), omega-like repressors (22 CvkRs), CopG-like repressors (11  
179 CvkRs) or unspecified HTH domain-containing proteins (8 CvkRs). The MerR family  
180 proteins, which also include Alr3614 (NCBI accession: BAB75313.1) from our model  
181 organism *Anabaena* 7120, range from 139 to 185 amino acids in length and appear to



182 be monophyletic (**Fig. 2**). Four CvkR proteins differed further in representing fusion  
183 proteins with an *hsdR*-restriction domain from a DNA-restriction-methylation (RM)  
184 system. RM systems are frequent among the CAST cargo genes, but there is no  
185 evidence that RM and CAST systems work together at a mechanistic level. The other  
186 HTH proteins are shorter (80-108 residues) and appear polyphyletic (**Fig. 2**). This  
187 indicates that these systems gather different regulators independent from one another.  
188 The shortest CvkRs are CopG-like proteins and Omega-like repressors containing an  
189 RHH DNA-binding domain and ranging from 53 to 72 amino acids in size. For instance,  
190 the second CvkR candidate in *Anabaena* 7120 encoded by *asl2690* (BAB74389.1)  
191 belongs to the CopG-like family (**Fig. 2** and **Table S1**). Proteins in both of these families  
192 can form homodimers, which create a joint antiparallel  $\beta$ -sheet as the basis for DNA  
193 binding<sup>20</sup>.

194

### 195 ***Expression of Alr3614 from leaderless mRNA***

196 The CvkR encoded by *alr3614* was annotated as a 168 amino acid-long MerR protein.  
197 However, sequence comparison of Alr3614 against other MerR-type CvkRs indicated  
198 that the NCBI annotation for this protein (here called CvkR-L) was too long (supported  
199 by 47 out of 50 homologs), and the actual protein would be 18 residues shorter (here  
200 called CvkR-S; **Fig. 3A**). Furthermore, the distance between *cas12k* and genes  
201 encoding CopG- and Omega-like CvkRs was longer than that between *cas12k* and  
202 genes encoding MerR-type CvkR proteins (usually <100 nt) (**Fig. 3B**).

203 Moreover, the start codon of *alr3614S* coincides with the previously mapped  
204 transcriptional start site (TSS) of its mRNA<sup>21</sup>, suggesting translation of CvkR-S from a  
205 leaderless mRNA. The TSS of *cas12k* coincides with the first nucleotide of the start  
206 codon as well; therefore, Cas12k is likely also translated from leaderless mRNA. Both  
207 genes and their TSSs are separated by an intergenic spacer of 82 nt in *Anabaena*



208 7120, and their homologs in other species are probably leaderless as well, judged by  
209 the generally shorter distance between the two genes than for other types of CvkR-  
210 encoding genes (**Fig. 3B**).

211 To verify the leaderless expression of CvkR-S, we constructed an *alr3614* deletion  
212 mutant ( $\Delta cvkR$ ) using the CRISPR-Cas12a (Cpf1) genome editing tool (**Fig. S1A and**  
213 **B**) and three versions of complementation mutants ( $\Delta cvkRCom-1$  to -3). For  
214 complementation, shuttle vectors were used, which carried *cvkR* genes driven by the  
215 copper-inducible *petE* promoter for the long form CvkR-L ( $\Delta cvkRCom-1$ ) or the short  
216 form CvkR-S, either containing a leader sequence ( $\Delta cvkRCom-3$ ) or not ( $\Delta cvkRCom-$   
217 2). For detection, a 3xFLAG epitope-encoding tag was fused to all three *cvkR* reading  
218 frames. The complementing plasmids were introduced into the  $\Delta cvkR$  deletion  
219 background and verified (**Fig. S1C and D**). The *cvkR* gene was transcribed in all three  
220 constructs (**Fig. 3C**). Translation of the encoded proteins was detected by Western  
221 blot, with clear size differences between CvkR-L and CvkR-S (**Fig. 3D**). Intriguingly, in  
222  $\Delta cvkRCom-1$ , we detected not only the CvkR-L form but also a small amount of CvkR-  
223 S, suggesting a propensity for initiation of translation at codon 18 even if the mRNA  
224 was 5' elongated. As there was no 5'UTR in  $\Delta cvkRCom-1$  following  $P_{petE}$ , it seems that  
225 the A in the start codon of CvkR-S could also serve as a start site of translation if  
226 combined with transcription from a strong promoter. The incongruence between *cvkR*  
227 mRNA and protein levels within  $\Delta cvkRCom-3$  implied that the 5'UTR of  $P_{petE}$  might  
228 impact the transcription rate, mRNA stability and/or translation efficiency of the *cvkR*-  
229 S mRNA. Taken together, we provide solid evidence that CvkR could be expressed  
230 from leaderless mRNA ( $\Delta cvkRCom-2$ ) or the start codon corresponding to codon 18 of  
231 the original annotation ( $\Delta cvkRCom-3$ ). Because the correct inducibility from the  $P_{petE}$

232 promoter was only observed in  $\Delta cvkR$ Com-2, we employed this strain for all  
233 subsequent complementation experiments, naming it henceforth  $\Delta cvkR$ Com.

234

### 235 ***Deletion of *alr3614* impacts *cas12k* and CRISPR array expression in vivo***

236 The AnCAST system contains all known associated genes and extends over  
237 approximately 21 kb (**Fig. 4A**). In addition to its core CAST components, it encodes  
238 multiple other transposases, possible regulators, a toxin/antitoxin pair, and an RM  
239 system. The *cas12k* gene (*alr3613*) lies upstream, reverse to *cvkR*. To analyze CvkR  
240 function *in vivo*, Northern hybridization of total RNA from triplicate clones of WT,  $\Delta cvkR$ ,  
241 and  $\Delta cvkR$ Com with single-stranded RNA probes was performed. Specific signals for  
242 *cvkR* mRNA were detected in  $\Delta cvkR$ Com (**Fig. 4B**). Northern hybridizations against  
243 tracrRNA and the AnCAST CRISPR array yielded signals <500 nt, which were strongly  
244 increased in  $\Delta cvkR$  compared to the wild-type control and strongly decreased in  
245 intensity in the complementation strain  $\Delta cvkR$ Com (**Fig. 4C, D**). We also detected an  
246 increased signal intensity for *cas12k* mRNA in  $\Delta cvkR$ , while the signal was below the  
247 detection limit in WT and  $\Delta cvkR$ Com (**Fig. 4E**), consistent with previous transcriptomic  
248 data (<sup>19</sup> and Bioproject PRJNA624132).

249 These data provide direct evidence that CvkR directly or indirectly regulates the  
250 abundance of tracrRNA promoter-derived transcript(s) and *cas12k* mRNA.

251 Moreover, the presence of longer transcripts indicated that tracrRNA and the CRISPR  
252 array are transcribed into a longer precursor that is subsequently processed into the  
253 major accumulating fragments of ~150 and ~200 nt, respectively. This is consistent  
254 with previous results of differential RNA-seq<sup>21</sup> and extensive transcriptome data<sup>19</sup> that  
255 suggested that the AnCAST CRISPR array would not have its own specific promoter.  
256 Instead, the joint tracrRNA-CRISPR array precursor is transcribed from a TSS that is

257 located 35 nt downstream of the *cas12k* coding sequence, at position 4,362,990 on  
258 the reverse strand, 413 nt upstream of the first repeat of the CRISPR array<sup>14</sup>.  
259 Nevertheless, it should be noted that the CRISPR array showed much more abundant  
260 signals in the  $\Delta cvkR$  deletion mutant compared to WT and  $\Delta cvkRCom$ , while *tracrRNA*  
261 was also well detectable in WT and  $\Delta cvkRCom$  (**Fig. 4C, D**). Thus, there are additional  
262 factors involved, likely acting on the processing and stabilization of array-derived  
263 transcripts.

264

### 265 ***Transcriptomic analysis of deletion mutant $\Delta cvkR$ and complementation strain*** 266 ***$\Delta cvkRCom$***

267 To investigate transcriptomic changes upon *cvkR* deletion, microarray analysis was  
268 performed using the  $\Delta cvkR$  and  $\Delta cvkRCom$  deletion and complementation strains.

269 After induction of *cvkR* transcription from the copper-inducible *petE* promoter, the  
270 mRNA levels and CvkR protein expression were verified in biological triplicate samples  
271 via Northern hybridization (**Fig. 5A**) and Western blot analysis (**Fig. 5B**). Hence, the  
272 absence or overexpression of CvkR in  $\Delta cvkR$  or  $\Delta cvkRCom$ , respectively, was  
273 confirmed, and the strains were investigated for further transcriptomic differences. The  
274 microarrays used cover all protein-coding genes as well as noncoding RNAs and were  
275 especially designed to allow the direct hybridization of labeled total RNA without prior  
276 conversion into cDNA<sup>22</sup>. Therefore, they enable the direct detection of *tracrRNA* and  
277 CRISPR array transcript levels. Microarray analysis revealed a small number of  
278 dysregulated genes. Thirteen features were significantly upregulated (7 protein-coding  
279 genes and 6 other transcripts) and 8 were significantly downregulated (6 protein-  
280 coding genes and 2 other transcripts) in  $\Delta cvkR$  compared to  $\Delta cvkRCom$  (**Fig. 5C**). In  
281 addition to the AnCAST genes *cas12k* and *tnsB* (*all3630*), the *tracrRNA* and CRISPR

282 array were upregulated (**Fig. 5D**) upon deletion of *cvkR*. Hence, the role of CvkR as a  
283 regulator of the AnCAST system was confirmed and further extended.

284 The dataset of all transcripts with meaningful fold changes is provided in **Table S2**, the  
285 raw data are available from the GEO database (<https://www.ncbi.nlm.nih.gov/geo/>)  
286 under the accession number GSE183629.

287

### 288 ***CvkR DNA binding and definition of the bound sequence***

289 To define the minimal necessary sequence and motifs required for CvkR binding, the  
290 promoter sequence of *cas12k* ( $P_{cas12k}$ ) was analyzed in a DNase I footprinting assay  
291 (**Fig. 6**). We first examined the binding activity of CvkR on a 287 bp DNA fragment  
292 covering the whole  $P_{cas12k}$  region in an electrophoretic mobility shift assay (EMSA).  
293 When providing equal amounts of this DNA fragment, it was with increasing  
294 concentrations of CvkR increasingly retarded (**Fig. 6A**, left panel). Then, we started to  
295 seek the CvkR binding region by further sequencing analysis. A specific area between  
296 15 and 57 nt upstream of *cas12k* was finally identified which exhibited significant CvkR-  
297 mediated protection (**Fig. 6A**, right panel). At higher CvkR concentrations, the area  
298 expanded further even downstream of the *cas12k* start codon, which could be a result  
299 of nonspecific DNA binding or CvkR dimerization. Other areas were unaffected by  
300 CvkR addition, which indicates a specific binding affinity at this location. Interestingly,  
301 the identified DNase-protected area overlaps with an inverted repeat (IR), 5'-  
302 AAAACACA-N21-TGTGTTTT-3' (**Fig. 6A**, right panel). To investigate this further, we  
303 also looked at other CAST systems with closely related *cvkR* genes (>70% sequence  
304 identity; **Fig. 2**) and compared their *cas12k* promoter regions, yielding six candidates.  
305 The sequences upstream of these six *cas12k* genes were aligned, and the -35 and -  
306 10 regions of  $P_{cas12k}$  and  $P_{cvkR}$  were predicted by the PromoterHunter program<sup>23</sup>. The  
307 alignment of these sequences showed that the IR motifs are conserved, surround the

308 -35 region of  $P_{cas12k}$  and overlap the -35 region of  $P_{cvkR}$  in all instances (**Fig. 6B**), which  
309 is also a typical feature of other MerR-controlled genes. Furthermore, this finding  
310 provided further support that the leaderless expression of *cas12k* and *cvkR* is  
311 conserved. Other promoters likely controlled by CvkR, such as  $P_{tnsB}$  and  $P_{tracr}$ , were  
312 also analyzed, but a closely related sequence was not found (**Fig. S2**).

313

### 314 ***TXTL assays verify CvkR repressor function***

315 To further delineate the relationship between CvkR and the promoter elements  
316 controlled by it, we tested the interaction of CvkR with different promoter fragments  
317 (**Fig. 7A**) using EMSAs and a cell-free transcription-translation system (TXTL<sup>24</sup>).

318 Recombinant CvkR was incubated at different concentrations with these fragments.

319 The full-length  $P_{cas12k}$  promoter yielded by far the strongest interaction, and band shifts  
320 could be seen at the lowest tested concentration of 0.5  $\mu$ M CvkR (**Fig. 7B**), indicating  
321 a high sensitivity for the CvkR:DNA interaction. The incubation with higher CvkR  
322 concentrations increased the signal intensity and showed a supershift or nonspecific  
323 DNA-binding affinity at the highest tested concentration of 5  $\mu$ M CvkR. All other  
324 fragments showed substantially weaker interactions, independent of sequence or  
325 fragment length (**Fig. 7B**).

326 To test these interactions independently, we cloned the full-length *cas12k* promoter  
327  $P_{cas12k}$  and several of the shorter promoter fragments upstream of a deGFP reporter  
328 gene to test whether they can drive transcription and thereby deGFP production in the  
329 TXTL assay<sup>24</sup>. In parallel, CvkR was expressed from a second plasmid (**Fig. 7C**).

330 The promoter of *cas12k* ( $P_{cas12k}$ ) was found to drive deGFP expression well (**Fig. 7D**).  
331 If CvkR was coexpressed, deGFP production was decreased to a value matching the  
332 baseline without added deGFP plasmid. P43, a 5' shortened variant of  $P_{cas12k}$ , yielded  
333 an ~30% lower deGFP fluorescence than the full-length promoter and was fully

334 repressed upon coexpression of CvkR (**Fig. 7D**). Thus, the 43 nt fragment in P43  
335 encompassing the -10 and -35 elements and one of the palindromes constitutes a  
336 minimal promoter. Further truncation of  $P_{cas12k}$  on the 3' and 5' ends (P39, P26, P20)  
337 substantially reduced promoter activity, but the activity could still be lowered by the  
338 parallel expression of CvkR (**Fig. 7D, E**).

339 Next, we tested the promoter driving tracrRNA transcription ( $P_{tracr}$ ) in the same system.  
340 We found that  $P_{tracr}$  yielded high deGFP expression, comparable to  $P_{cvkR}$ , and that the  
341 expression was abolished in the presence of native CvkR (**Fig. 7F**). The promoter of  
342 *cvkR* ( $P_{cvkR}$ ) was not able to drive deGFP transcription in the TXTL system (**Fig. 7F**).  
343 Therefore, whether CvkR can regulate its own transcription could not be tested in this  
344 assay.

345

### 346 ***The crystal structure reveals that CvkR is a new type MerR-type regulator***

347 The results shown in **Figs. 4 to 7** established CvkR as a repressor of the AnCAST  
348 system. To investigate CvkR functionality at the structural level, a high-quality crystal  
349 structure was solved at 1.5 Å resolution by using the single-wavelength anomalous  
350 dispersion (SAD) method (detailed data are in **Table S3**). A clear electron density of  
351 the added ATP molecule used in the optimization of crystallization appeared at the  
352 proposed effector-binding domain of CvkR (**Fig. 8**). However, despite our best  
353 endeavors on the apo CvkR structure, the crystal quality was insufficient for diffraction  
354 data collection. The failure might result from the high flexibility of the C-terminus without  
355 its bound effector.

356 The solved structure shows that there is one CvkR monomer binding one ATP  
357 molecule in the crystallographic asymmetric unit (ASU) (PDB ID code 7XN2, **Fig. 8A**).  
358 Further analysis through PDBePISA shows that the interface area between two

359 adjacent CvkR monomers is as high as 970.1 Å, suggesting that CvkR forms stable  
360 homodimers in solution (**Fig. 8B**), consistent with the results of size exclusion  
361 chromatography (**Fig. S3**). Both analyses collectively indicated that CvkR functions as  
362 a homodimer similar to other reported members of the MerR family.

363 The overall structure of the CvkR monomer consists of a classical wHTH DNA-binding  
364 domain at the N-terminus (residues 1-80), a novel dimerization domain (residues 81-  
365 132), and a potential effector-binding helix in the C-terminal region (helix  $\alpha 7$ , residues  
366 133-150), in which a clear ATP ligand is bound (**Fig. 8A and B**). The topology of the  
367 DNA-binding domain is typical  $\alpha 1$ - $\alpha 2$ -W1- $\alpha 3$ -W2- $\alpha 4$ , which contains four  $\alpha$ -helices and  
368 two wings and is largely preserved in the MerR-like superfamily. The classical wHTH  
369 domain structure in the CvkR N-terminus, combined with the results of our TXTL,  
370 EMSA and transcriptome analyses, confirms that CvkR belongs to the MerR-type  
371 family of transcriptional regulators. However, the dimerization domains in our solved  
372 structure differ from the existing reported MerR family members (**Fig. 8C**). Instead of  
373 dimerizing the antiparallel coiled coil formed by two longer, central  $\alpha$ -helical linkers,  
374 CvkR dimerizes via three antiparallel  $\beta$ -strands ( $\beta 2$ - $\beta 1$ - $\beta 3$ ) and one short  $\alpha$ -helix ( $\alpha 6$ )  
375 from the two protomers in the dimer (**Fig. 8B and C**). This is a completely new folding  
376 pattern of dimerization among the MerR family members reported thus far, indicating  
377 that CvkR is a structurally novel MerR-type protein.

378 It is well known that the C-terminal domain of MerR family regulators is responsible for  
379 specifically recognizing effector and sensing signals and ranges in size from a few  
380 residues to hundreds of amino acids. In general, the larger C-terminal domain is  
381 composed of multiple secondary structure elements and is often involved in multidrug  
382 resistance. In contrast, the shorter C-terminal domains, such as CueR and SoxR,  
383 mostly display a short  $\alpha$ -helix structure (**Fig. 8C**) and function as bacterial sensors of  
384 metal ions or oxidative stress with the help of a conserved cysteine residue. According



385 to the size of the C-terminal domain, CvkR belongs to the latter group; however, it lacks  
386 the conserved cysteine motif (at position 134, **Fig. S4**) and binds an ATP molecule  
387 (**Fig. 8C**). These features again indicate the novelty of CvkR in structure and function.  
388 Interestingly, the ATP ligand, used at the crystal optimization stage to obtain high-  
389 quality crystals for diffraction data collection, binds exactly to the putative effector-  
390 binding domain of CvkR (**Fig. 9**). The efficient binding of the adenine moiety is  
391 achieved through  $\pi$ - $\pi$  stacking contributed by several aromatic residues, a cation- $\pi$   
392 interaction provided by R136, and specific hydrogen bonding patterns (**Fig. 9A**).  
393 Notably, the hydrophobic residue W133, originally embedded in the hydrophobic  
394 interior, is exposed to the solution side due to the binding of ATP, implying that some  
395 conformational changes in this region may occur with ATP binding. These interactions  
396 indicate a certain degree of base-recognition specificity, but we cannot draw a  
397 conclusion that it is adenine-specific due to the large number of water molecules  
398 participating in the formation of a hydrogen bond interaction network. The two hydroxyl  
399 groups of the ribose moiety of ATP separately formed hydrogen bonds with the side  
400 chain of residue Q140 and a water molecule. Although the interaction between Q140  
401 and the ribose moiety also presents some specificity, the recognition specificity of this  
402 site is obviously less than that of the adenine-binding site. In contrast, the triphosphate  
403 group of ATP is free outside the CvkR molecule in our solved structure, suggesting  
404 that the ATP molecule is not the actual effector of CvkR. These findings point to an  
405 effector molecule that may be related to the cyclic oligonucleotide family of signaling  
406 molecules observed in certain types of CRISPR-Cas and other defense systems<sup>25,26</sup>,  
407 but attempts testing several commercially available candidates remained inconclusive.  
408 Further structural analysis revealed that the triphosphate group of ATP was inserted  
409 into the wHTH DNA-binding domain of the adjacent CvkR' molecule and interacted  
410 with W1 and helix  $\alpha$ 1 (**Fig. 9B and C**). W1 in the wHTH DNA-binding domain has been

411 proven to be involved in the binding of MerR family members to the phosphate  
412 backbone of DNA. Different from the relatively nonspecific interaction between the  
413 triphosphate group and the main chains of other residues, the side chain of residue  
414 R42 in the W1 region forms specific hydrogen bonds with the phosphate group,  
415 implying that R42 is likely to participate in the binding of CvkR to DNA (**Fig. 9C**).  
416 Therefore, the solved CvkR-ATP complex indirectly proves that CvkR binds to nucleic  
417 acids through the wHTH domain.

418 In terms of DNA recognition, MerR regulators generally utilize residues in their  $\alpha$ 2-helix  
419 to engage the major groove, while residues in their wings of the wHTH domain engage  
420 the minor groove in the target DNA. However, the crystal quality of the CvkR-DNA  
421 complex was insufficient for diffraction data collection. Thus, we superposed our solved  
422 CvkR structure onto other reported MerR regulator-promoter complex structures.  
423 Structural comparison suggests that  $\alpha$ 2-helix residues R19, R20, Q21, Q23, Y24, R26  
424 and E27 insert into the DNA major groove, W1 loop residues K40, R42, N43 and V44  
425 insert into the DNA minor groove, and W2 loop residues N66, F67 and D68 are close  
426 to the DNA phosphate backbone. Except for residues R19, R26, K40, R42 and N43,  
427 the mentioned residues correspond to residues in HiNmIR, which have been found to  
428 be involved in DNA binding<sup>27</sup>.

429 To verify the relevance of these residues for transcriptional regulation, mutagenesis  
430 and TXTL functional assays were performed (**Fig. 10**). Six amino acids were changed  
431 to alanine (R19A-R20A-Q23A-K40A-R42A-N66A), and the resulting variant protein  
432 was called CvkRmut. Both CvkR and CvkRmut were stably produced in the TXTL  
433 assay (**Fig. 10A**). Similar to the assay shown in **Fig. 7**, the promoter of *cas12k* ( $P_{cas12k}$ )  
434 was found to drive deGFP expression well (**Fig. 10B**). If CvkR was coexpressed (1 nM,  
435 2.5 nM or 5 nM) with  $P_{cas12k}$ -driven deGFP production, GFP fluorescence decreased  
436 to a value matching the baseline without added deGFP plasmid (**Fig. 10C**). This effect

437 was observed at the lowest amount of added plasmid used, 1 nM. Therefore, CvkR  
438 was able to completely repress deGFP expression driven from  $P_{cas12k}$  at low  
439 concentrations.

440 In contrast, CvkRmut expressed from the 1 nM plasmid could not repress  $P_{cas12k}$ -driven  
441 deGFP expression as efficiently as CvkR. However, if a higher amount of 5 nM plasmid  
442 was added, CvkRmut was able to repress deGFP almost to the same level as CvkR  
443 expressed from 1 nM plasmid (**Fig. 10C**). These results indicated that CvkRmut was a  
444 mild binding-deficient mutant that was still functional but not as efficient as the native  
445 CvkR, hence supporting the predicted functional relevance of these residues.

446

## 447 **Discussion**

448 Native type V-K CAST systems have thus far only been found in certain  
449 cyanobacteria<sup>11,14</sup>. Their better characterization is of fundamental interest, and these  
450 systems hold great promise for the development of novel genome editing tools<sup>28</sup>. The  
451 primary function of native CRISPR-Cas systems is defense against mobile genetic  
452 elements. Therefore, we reasoned that the activity of CAST systems that can  
453 transpose to novel sites within a genome must be controlled. Here, we first addressed  
454 the association between putative transcriptional regulators and cyanobacterial CAST  
455 systems and found four different classes of such repressors, which we suggest to  
456 name CvkR, for Cas-type V-K repressors. The consistent occurrence of these  
457 regulators in 94 of 118 analyzed systems indicates a functional dependency. Judged  
458 by the diversity of regulators and their DNA-interference domains, CvkRs likely have  
459 originated several times independently.

460 We then characterized the transcriptional regulator of the AnCAST system of  
461 *Anabaena* 7120 encoded by gene *alr3614* in detail. Our data show that CvkR controls

462 the expression of the AnCAST core module (i.e., *tracrRNA*, *cas12k* and *tnsB*, *tnsC* and  
463 *tniQ* mRNAs).

464 The crystal structure analysis revealed specific features within the dimerization and  
465 effector-binding domains of CvkR that were previously unknown for members of the  
466 MerR-type family of transcription factors. The MerR family was first discovered as a  
467 regulator of mercury resistance operons<sup>29,30</sup> but is also involved in multiple cell  
468 functions, such as drug resistance, responses to heavy metals and protection against  
469 oxidative stress<sup>31–33</sup>. In gram-negative bacteria, transposable elements such as Tn21  
470 and Tn501 frequently contain mercury resistance (*mer*) operons, which are controlled  
471 by transcription factors belonging to the MerR family.

472 MerR regulators typically contain an N-terminal HTH domain followed by a dimerization  
473 helix and an effector-binding domain at the C-terminus<sup>29,34</sup>. The protein forms a coiled-  
474 coil homodimer facilitated over the dimerization helix and is able to bind a palindromic  
475 DNA motif<sup>35</sup>. The protein can bind DNA with and without effector binding, which leads  
476 to the protein functioning as either an activator or a repressor. The palindromic binding  
477 region is usually inside promoters with an elongated distance (>19 nt) between the -10  
478 and -35 elements, so MerR represses the binding of the  $\sigma$ -factor<sup>29</sup>. This is also true for  
479 the AnCAST system and CvkR, in which the distances between the -35 and -10  
480 elements are 21 nt for the *cas12k* promoter (**Fig. 6B**) and 19 nt for the P<sub>tracr</sub> promoter.  
481 In contrast, this distance is 17 nt for the *cvkR* and *tnsB* (*all3630*) promoters.

482 Effector binding, however, can trigger a conformational change, which brings both HTH  
483 domains closer together and distorts the DNA to increase the  $\sigma$ -factor affinity for the  
484 promoter<sup>29,35</sup>. The effector for this regulator is usually a metal ion, but there are also  
485 MerR interactions with antibiotics, oxidative stress, or lipophilic compounds<sup>29,36–38</sup>.  
486 MerR-like proteins without effector interactions are also known<sup>39</sup>.

487

488 No fluorescence was observed if CvkR was coexpressed in a cell-free transcription-  
489 translation system (TXTL) together with deGFP reporter gene fusions of the *cas12k*  
490 promoter  $P_{cas12k}$  and the tracrRNA promoter  $P_{tracr}$ , while in the absence of CvkR, strong  
491 signals were detected (**Fig. 7**). These results establish CvkR as a transcriptional  
492 repressor of the AnCAST system. We tested mutated versions of the protein and of  
493 the promoter sequence, yielding insight into the functionality of the protein as a dimeric  
494 HTH-domain-containing transcriptional repressor and allowing delineation of the  
495 binding motif at the DNA level. The genome-wide analysis of transcriptomic effects  
496 yielded, in addition to the three CvkR-controlled promoters shown in **Fig. 7F**, evidence  
497 for further promoters possibly under its control, both on the chromosome and on  
498 plasmids  $\alpha$  and  $\delta$  (**Fig. 5C** and **Table S2**). MerR-type regulators are principally better  
499 known as transcriptional activators rather than transcriptional repressors. Our data  
500 show that transcription of three promoters in the AnCAST system was enhanced in the  
501  $\Delta cvkR$  mutant. While we detected the repressor function as the default mechanism,  
502 we speculate that this interaction might become lost in the presence of a bound effector  
503 molecule.

504 Genes upregulated in  $\Delta cvkRCom$  (**Fig. 5C**) include a set of 26 tRNA genes on the  $\delta$   
505 plasmid. These were recently identified as an L-array that became specifically induced  
506 when cultures were exposed to sublethal concentrations of ribosome-targeting  
507 antibiotics<sup>40</sup>. Moreover, the adjacent gene *all8564* encoding an HNH-type homing  
508 endonuclease and the chromosomal gene *all3626* (*rtcB*) were found to be coregulated.  
509 Therefore, the genes that were significantly more highly expressed in  $\Delta cvkRCom$   
510 indicated the presence of translational stress due to the presence of antibiotics.

511  
512 Structural analysis of CvkR at 1.5 Å resolution yielded elements typical for a member  
513 of the MerR-type transcription factor family but with distinct dimerization and effector-

514 binding domains. In particular, the 28 Å and 54 Å distances between two  $\alpha$ 2-helices  
515 and two W1 loops in CvkR, covering ~9 bp and ~17 bp, respectively, in B-form DNA,  
516 are both obviously shorter than those in the HiNmIR-promoter complex (35 Å/74 Å;<sup>27</sup>)  
517 and other reported MerR regulator-promoter complexes, such as SoxR (35 Å/74 Å)  
518 and the activator CopA (35 Å/65 Å) (**Fig. 8B**). The  $\alpha$ 2-helix in the wHTH DNA-binding  
519 domain is well known for base-specific recognition by MerR-type transcriptional  
520 regulators. Individual MerR-family homodimer proteins bind specifically to the two half-  
521 sites of quasi-palindromic inverted repeat (IR) DNA sequences within the target gene  
522 promoter via its two  $\alpha$ 2-helices. This is compatible with the length of one IR half-site  
523 recognized by CvkR of 8 bp (**Fig. 6B**).

524

525 To summarize, we identified and characterized CvkR as the regulator of the AnCAST  
526 system and found that it may impact a small set of host genes. Structural analysis of  
527 CvkR revealed that it is a structurally novel type of MerR protein because it dimerizes  
528 via three antiparallel  $\beta$ -strands and one short  $\alpha$ -helix ( $\alpha$ 6) (**Fig. 8B and C**). CvkR  
529 exhibits an effector-binding domain in its C-terminal region (**Fig. 9**), and the efficient  
530 binding of an adenine moiety points to a metabolite that may be related to the cyclic  
531 oligonucleotide family of signaling molecules observed in certain types of CRISPR-Cas  
532 systems<sup>25</sup>, as well as other antiphage signaling systems<sup>26</sup>. However, the exact effector  
533 molecule and the functionality of this hypothetical signaling input sensed by CvkR are  
534 matters of further research.

535

## 536 **Materials and methods**

### 537 ***Cultures of cyanobacteria and construction of mutant strains***

538 *Anabaena* 7120 and its derivatives were grown photoautotrophically in BG11 liquid  
539 medium or on agar plates under white light illumination of 30-50  $\mu\text{mol photons m}^{-2} \text{s}^{-1}$   
540 at 30 °C<sup>41</sup>. In terms of the strains for the control group in copper-inducible experiments,  
541 transparent plastic tissue culture flasks were used for cultivation, deionized water was  
542 used for medium preparation, and three resuspensions with copper-free medium were  
543 employed for the seed culture. In addition, excess  $\text{CuSO}_4$  (1.0 or 1.25  $\mu\text{M}$ ) was added  
544 to guarantee  $P_{petE}$  activity for the respective experiments. The culture was  
545 supplemented with erythromycin (10  $\mu\text{g/mL}$ ) when necessary.

546 For construction of  $\Delta alr3614$  ( $\Delta cvkR$ ), the CRISPR-Cas12a (Cpf1) genome editing tool  
547 together with the pSL2680 plasmid (Addgene No. 85581) were used as previously  
548 described<sup>19</sup>. The primer pair *alr3614gRNA-1/2* was used to prepare the gRNA-cassette  
549 editing plasmids, and the primer pairs *alr3614KO-1/2* and *alr3614KO-3/4* were used to  
550 prepare the gRNA & repairing-cassette editing plasmids. The primer pairs *alr3614-3/4*  
551 were used to check the deletion genotype. A 200 bp internal fragment  
552 (4365123~4365322) of *cvkR* was ultimately deleted.

553 For complementation of the  $\Delta cvkR$  mutant and/or verification of leaderless expression  
554 of the *cvkR* gene, three cassettes ( $P_{petE\_no\ 5'UTR}\text{-}alr3614L\text{-}3xFLAG$ ,  $P_{petE\_no\ 5'UTR}\text{-}$   
555  $alr3614S\text{-}3xFLAG$  and  $P_{petE}\text{-}alr3614S\text{-}3xFLAG$ ) were cloned into a shuttle vector  
556 (pRL59EH) derived from the broad-host-range plasmid RSF1010 by seamless  
557 assembly. The primer pairs 59M-F/59M-R1,  $P_{petE}\text{-}F/P_{petE}\text{-}R4$  and 3614L-F/3614-R  
558 were used to construct a complementation plasmid to generate  $\Delta cvkRCom\text{-}1$ . The  
559 primer pairs 59M-F/59M-R1,  $P_{petE}\text{-}F/P_{petE}\text{-}R5$  and 3614S-F1/3614-R were used to  
560 construct a complementing plasmid to generate  $\Delta cvkRCom\text{-}2$ . The primer pairs 59M-



561 F/59M-R1,  $P_{petE}$ -F/ $P_{petE}$ -R6 and 3614S-F2/3614-R were used to construct a  
562 complementing plasmid to generate  $\Delta cvkR$ Com-3. Each complementing plasmid was  
563 introduced into the  $\Delta cvkR$  mutant by conjugal transfer as previously reported<sup>42</sup>.  
564 Genotypes of mutants were confirmed by PCR (**Fig. S1**). The sequences of all  
565 oligonucleotides are listed in **Table S4**. All PCR fragments, plasmids generated in this  
566 study, and gene mutation regions in the mutants were verified by Sanger sequencing.  
567

### 568 ***Microarray analysis***

569 *Anabaena* 7120 strains  $\Delta cvkR$  and  $\Delta cvkR$ Com were grown in 50 mL BG11 without  
570  $CuSO_4$  to an  $OD_{750}$  of 0.8, and CvkR expression was induced from  $P_{petE}$  with 1.25  $\mu M$   
571  $CuSO_4$  for 24 h. Cells were harvested, and RNA was extracted as described<sup>19</sup>.  
572 The RNA samples of two biological replicates each were hybridized to 8x44K  
573 microarrays (Agilent ID 062842) following published sample preparation and  
574 hybridization details<sup>43</sup>. In short, 2  $\mu g$  of DNase-treated RNA was used for Cy3 labeling  
575 (ULS Fluorescent Labeling Kit for Agilent Arrays, Kreatech). Microarray hybridization  
576 was performed with 600 ng Cy3-labeled RNA for 17 h at 65 °C. Microarray raw data  
577 were processed with R software as described<sup>22</sup>. A  $|\log_2 FC| \geq 1$  threshold and a p value  
578  $\leq 0.01$  were considered to indicate a significant change in gene expression. The full  
579 dataset is accessible in the GEO database (<https://www.ncbi.nlm.nih.gov/geo/>) with  
580 the accession number GSE183629.

581

### 582 ***Northern blot analysis of mutants***

583 RNA isolation was performed using a Precellys 24 Dual homogenizer (Bertin) for cell  
584 lysis as previously described<sup>19</sup>. Twenty micrograms of total RNA were separated on  
585 10% polyacrylamide-8.3 M urea gels. CRISPR-related transcript accumulation was

586 analyzed by Northern hybridization using single-stranded radioactively labeled RNA  
587 probes transcribed *in vitro* from PCR-generated templates (see **Table S4** for primers),  
588 as previously described<sup>44</sup>.

589

### 590 ***Western blot analysis***

591 Cyanobacterial cell harvesting and protein extraction were performed as previously  
592 described<sup>45</sup>. Total proteins extracted from the samples were separated by 15% SDS–  
593 PAGE according to the standard procedure and electroblotted onto PVDF or  
594 nitrocellulose (NC) membranes. To check for equal loading, the membrane was  
595 stained with Ponceau S (0.1% (w/v) in 5% acetic acid). After destaining, the PVDF  
596 membranes were blocked in 3% skimmed milk-TBST (0.05% Tween-20 in TBS) at  
597 room temperature for 30 min. Then, the membranes were incubated with anti-3xFLAG  
598 tag monoclonal antibodies for 1 h and washed three times with TBST (15 min each).  
599 After that, the membranes were incubated with an alkaline phosphatase-linked  
600 secondary antibody for 1 h and washed three times with TBST (15 min each). Finally,  
601 signals were detected with the NBT (nitro-blue tetrazolium chloride) and BCIP (5-  
602 bromo-4-chloro-3'-indolyphosphate p-toluidine salt) methods. Methods for Western  
603 blot analysis of TXTL samples were used as described<sup>19</sup>.

604

### 605 ***Quantitative real-time PCR***

606 Total RNA extraction, removal of the genomic DNA and reverse transcription were  
607 performed using a Bacteria RNA Extraction Kit and HiScript III RT Supermix for qPCR  
608 (+gDNA wiper) kit (Vazyme) according to the manufacturer's instructions. SYBR  
609 Premix ExTaq™ (Takara, Dalian, China) was used for qRT–PCR, and the cycle  
610 thresholds were determined using a Roche LightCycler® 480 II sequence detection  
611 system (Roche, Shanghai, China). *mnpB* (RNase P subunit B) was used as the internal

612 control. The primers for *alr3614* (*cvkR*) and *rnpB* are listed in **Table S4**. Three  
613 independent experiments were performed, which showed consistent results.

614

### 615 ***TXTL assays***

616 To test promoter fragments in a cell-free transcription-translation system, the *E. coli*-  
617 based TXTL assay was used<sup>24,46</sup>. The myTXTL Sigma 70 Cell-Free Master Mix was  
618 purchased from Arbor Biosciences. The included p70a plasmid was used as a template  
619 for cloning of the promoter sequences  $P_{tracr}$ ,  $P_{cvkR}$ , and  $P_{cas12k}$  (**Fig. 7B**) in an open  
620 reading frame with the destabilized enhanced GFP (deGFP) and its 5'UTR. All PCRs  
621 were performed using PCRBio HiFi polymerase (PCR Biosystems). Promoter  
622 sequences were PCR-amplified from genomic DNA of *Anabaena* 7120 with overlaps  
623 to p70a. The p70a plasmid was also PCR-amplified.

624 The CvkR protein (Alr3614) and a mutant with potential reduced DNA-binding affinity  
625 (R16A-R20A-Q23A-K40A-R42A-N66A) (CvkRmut) were used for analysis in the TXTL  
626 assay. The *cvkR* sequence was PCR-amplified from genomic DNA of *Anabaena* 7120.  
627 The corresponding DNA fragment for CvkRmut was ordered from IDT as gBlocks and  
628 subcloned into pJet1.2/blunt (Thermo Fisher Scientific) and then amplified via PCR  
629 with overhangs to pET28a. The plasmid pET28a was PCR-amplified as well. The CvkR  
630 and CvkRmut proteins were thus expressed from an IPTG-inducible T7 promoter with  
631 an N-terminal 6xHis tag and a TEV site for potential cleavage of the tag.

632 Fragment assembly via AQUA cloning was performed at room temperature for 30 min  
633 upon transformation into chemically competent *E. coli* DH5 $\alpha$  cells for cloning.  
634 Assembled plasmids were isolated, and regions of interest were sequenced (Eurofins  
635 Genomics).

636 For the expression of proteins encoded on pET28a in the TXTL assay, T7 RNA  
637 polymerase (RNAP), expressed in this instance from p70a, and IPTG are necessary.

638 Reactions were performed in duplicate overnight at 29 °C in a total volume of 5 µL with  
639 3.75 µL of TXTL master mix, 1 mM IPTG, 0.5 nM p70a\_T7\_RNAP, 1 to 5 nM  
640 pET28a\_CvkR or CvkRmut and 2-5 nM p70a\_promoter\_deGFP. The fluorescence of  
641 deGFP was measured every 10 min (excitation 485 nm, emission filter 535 nm) in a  
642 plate reader (Wallac 1420 Victor<sup>2</sup> microplate reader from Perkin Elmer). Western blot  
643 analysis of TXTL samples was performed as described<sup>19</sup>.

644

#### 645 ***Heterologous expression and purification of CvkR protein***

646 For heterologous expression of CvkR in *E. coli*, the protein-coding sequence of CvkR  
647 was PCR-amplified from *Anabaena* 7120 genomic DNA and cloned into the pET28a-  
648 smt3 vector by using BamHI and XhoI restriction sites to generate the pET28a-  
649 smt3\_CvkR expression plasmid, which expresses CvkR with an Ulp1-cleavable N-  
650 terminal 6xHis-smt3 fusion tag. The used primers are listed in **Table S4**. The  
651 sequence-verified plasmid was then transformed into *E. coli* BL21(DE3) for protein  
652 expression.

653 The expression strain was grown in LB medium to approximately OD<sub>600</sub>~0.6 at 37 °C  
654 and induced at 25 °C overnight with 0.4 mM IPTG (isopropyl β-D-  
655 thiogalactopyranoside). After induction, cells were harvested by centrifugation and  
656 lysed in lysis buffer A (20 mM Tris-HCl, pH 8.0, 300 mM NaCl, 10 mM imidazole, 2 mM  
657 β-mercaptoethanol, 20 µg/mL DNase I) using a high-pressure homogenizer. After  
658 centrifugation at 20,000x g for 50 min, the supernatants were loaded onto a Ni  
659 Sepharose 6 FF column (GE Healthcare), washed with lysis buffer A containing 40 mM  
660 imidazole, and eluted with 20 mM Tris-HCl, pH 8.8, 300 mM imidazole, and 2 mM β-  
661 mercaptoethanol. The eluted fractions were treated with Ulp1 protease overnight at  
662 4 °C and purified with a Hitrap Heparin HP column (GE Healthcare) to remove the  
663 6xHis-smt3 fusion tag and impurities. Subsequently, tag-removed target protein

664 fractions were further purified by Superdex 200 Increase 10/300 GL (GE Healthcare).  
665 Finally, target proteins were collected, concentrated and stored in 10 mM Tris-HCl (pH  
666 8.8), 100 mM NaCl, and 2 mM  $\beta$ -mercaptoethanol.  
667 Selenomethionine-labeled (Se-Met) CvkR protein was overexpressed and purified  
668 using the same procedures described above; however, the medium was substituted  
669 with 1x M9 medium, and seven essential amino acids were added at the mid-log phase  
670 before induction. To prevent oxidation of the selenium atoms, 5 mM  $\beta$ -mercaptoethanol  
671 was added to the final elution fraction containing Se-Met CvkR.

672

### 673 ***Analysis of CvkR oligomeric forms in solution***

674 Size exclusion chromatography was performed with 0.3 mg CvkR at room temperature  
675 to probe the molecular weight of CvkR in solution. The Superdex 200 increase 10/300  
676 GL column was calibrated with a gel filtration calibration kit HMW (GE Healthcare) in a  
677 buffer containing 10 mM Tris-HCl (pH 8.8), 100 mM NaCl, 2 mM  $\beta$ -mercaptoethanol.  
678 The calibration curve based on the molecular markers is  $\log M_r = -0.20945V_e + 7.712$   
679 ( $R^2 = 0.9949$ ,  $V_e$ : elution volume;  $M_r$ : molecular weight).

680

### 681 ***EMSA analysis***

682 Each DNA duplex for EMSA was created by annealing two complementary  
683 oligonucleotides. The EMSA reaction (10  $\mu$ L) was carried out at room temperature by  
684 mixing 0.5  $\mu$ M DNA duplex and increasing concentrations of CvkR protein in binding  
685 buffer (50 mM Tris-HCl, pH 8.0, 100 mM KCl, 2.5 mM  $MgCl_2$ , 0.2 mM DTT, 10%  
686 glycerol). After incubation for 30 min, the reaction samples were electrophoresed on  
687 an 8% polyacrylamide gel with 0.5x TBE, and the gel was visualized by ethidium  
688 bromide staining.

689

690 ***DNase I footprinting assays***

691 DNase I footprinting assays were carried out similar to previous research<sup>47</sup>.  
692 Specifically, ~300 nt FAM-labeled probes, including an 82 nt intergenic spacer between  
693 the *cas12k* and *cvkR* genes, were PCR amplified with 2x TOLO HIFI DNA polymerase  
694 premix (TOLO Biotech, Shanghai) using primers P3613-F(FAM) and P3613-R and  
695 purified by the Wizard® SV Gel and PCR Clean-Up System (Promega, USA). Binding  
696 reactions were performed in a total volume of 40 µL containing 50 mM Tris-HCl, pH  
697 8.0, 100 mM KCl, 2.5 mM MgCl<sub>2</sub>, 0.2 mM DTT, 10% glycerol, 2 µg salmon sperm DNA,  
698 300 ng probes and 0.1 µg CvkR protein at room temperature for 30 min. Following  
699 DNase I treatment (Promega), phenol/chloroform extraction, and ethanol precipitation,  
700 products were dissolved in 30 µL MiniQ water. The preparation of the DNA ladder,  
701 electrophoresis and data analysis were the same as described before<sup>47</sup>, except that  
702 the GeneScan-LIZ600 size standard (Applied Biosystems) was used.

703

704 ***Phylogenetic analysis of CvkR***

705 The identified CvkR proteins were compared to each other and analyzed for alternative  
706 start positions to correct potential incorrect annotations, as in the case of CvkR  
707 (Alr3614, BAB75312.1). Elongated N-terminal regions with no similarity to homologs  
708 encoded by other *cvkR* genes were removed from the analysis. The sequences were  
709 then aligned by M-coffee<sup>48,49</sup> and further analyzed by the BEAST algorithm<sup>50</sup>. The  
710 phylogenetic analyses were calculated by the Yule process (speciation), the  
711 substitution model Blosum62 and MCMC chain length of 1e6 to log parameters every  
712 1e3 steps<sup>51–53</sup>.

713

714 ***Crystallization, data collection, and structure determination of the CvkR protein***

715 Using a hanging drop-vapor diffusion method, both native and selenomethionine-  
716 substituted (Se-Met) CvkR crystals appeared at 18 °C in crystallization reagent  
717 containing 0.1 M phosphate citrate (pH 4.4~4.6) with 15%~20% PEG300. However,  
718 diffraction-quality crystals were obtained only when 10 mM ATP was added into the  
719 crystal screen droplet, which consisted of a 1:1 (v/v) protein at 15 mg/mL and the well  
720 crystallization reagent. Before flash cooling in liquid nitrogen, crystals were cryo-  
721 preserved using crystallization reagent supplemented with 15% PEG400.

722 The diffraction data were collected at the Shanghai Synchrotron Radiation Facility  
723 (SSRF), beamlines BL17U1 and BL18U1, in a 100K nitrogen stream. Data indexing,  
724 integration, and scaling for native CvkR were conducted using HKL3000 software<sup>54</sup>.  
725 SAD X-ray diffraction data were processed by Aquarium software<sup>55</sup>. The resulting main  
726 chain structure was used as the initial search model for molecular replacement by  
727 Phaser to determine the native CvkR structure<sup>56</sup>. Structure refinements were iteratively  
728 performed using the programs Phenix and Coot<sup>57,58</sup>. The statistics for data processing  
729 and structure refinement are shown in **Table S3**. The coordinates were deposited in  
730 the Protein Data Bank with the PDB ID code 7XN2. Figures were prepared using  
731 PyMOL<sup>59</sup>.

732

### 733 **Data availability**

734 The full transcriptome datasets for the WT and mutants  $\Delta cvkR$  and  $\Delta cvkRCom$  are  
735 accessible from the GEO database (<https://www.ncbi.nlm.nih.gov/geo/>) with the  
736 accession number [GSE183629](#). The structural data can be accessed at the Protein  
737 Data Bank (<https://www.rcsb.org/>) under the PDB accession number 7XN2.

738



739 **Funding**

740 Financial support for this work was provided by the National Key Research and  
741 Development Program of China (Grant number 2021YFA0909700), the Joint Sino-  
742 German Research Program (grant HE 2544/13-1 to WRH and grant M-0214 to XL),  
743 the DFG (grant HE 2544/14-2 to WRH), the National Natural Science Foundation of  
744 China (Grant numbers 31525002, 31570068 and 31761133008), the QIBEBT and  
745 Dalian National Laboratory for Clean Energy (DNL), CAS (grant QIBEBT I201904 to  
746 TZ), and the Shandong Taishan Scholarship (to XL).

747

748 **Author contributions**

749 WRH, XL and TZ designed the study. TZ, YX and HL constructed the *Anabaena* 7120  
750 mutant strains. VR performed the TXTL experiments, microarray analyses and  
751 Northern hybridizations. MZ did the majority of bioinformatic analyses. YS and YX  
752 performed the qRT-PCR and Western blot analyses. YL performed the structural  
753 analysis of CvkR. VR, MZ, YL, TZ and WRH wrote the paper with contributions from  
754 all authors.

755

## 756 **References**

- 757 1. Bhaya, D., Davison, M. & Barrangou, R. CRISPR-Cas systems in Bacteria and  
758 Archaea: versatile small RNAs for adaptive defense and regulation. *Ann. Rev Gen.*  
759 **45**, 273–297 (2011).
- 760 2. Grissa, I., Vergnaud, G. & Pourcel, C. The CRISPRdb database and tools to display  
761 CRISPRs and to generate dictionaries of spacers and repeats. *BMC Bioinformatics*  
762 **8**, 172 (2007).
- 763 3. Jansen, R., Embden, J. D. A. van, Gaastra, W. & Schouls, L. M. Identification of  
764 genes that are associated with DNA repeats in prokaryotes. *Mol. Microbiol.* **43**,  
765 1565–1575 (2002).
- 766 4. Lange, S. J., Alkhnbashi, O. S., Rose, D., Will, S. & Backofen, R. CRISPRmap: an  
767 automated classification of repeat conservation in prokaryotic adaptive immune  
768 systems. *Nucleic Acids Res.* **41**, 8034–8044 (2013).
- 769 5. Makarova, K. S. *et al.* An updated evolutionary classification of CRISPR-Cas  
770 systems. *Nat. Rev. Microbiol.* **13**, 722–736 (2015).
- 771 6. Hochstrasser, M. L. & Doudna, J. A. Cutting it close: CRISPR-associated  
772 endoribonuclease structure and function. *Trends Biochem. Sci.* **40**, 58–66 (2015).
- 773 7. Knott, G. J. & Doudna, J. A. CRISPR-Cas guides the future of genetic engineering.  
774 *Science* **361**, 866–869 (2018).
- 775 8. Hidalgo-Cantabrana, C., Goh, Y. J. & Barrangou, R. Characterization and  
776 Repurposing of Type I and Type II CRISPR–Cas Systems in Bacteria. *J. Mol. Biol.*  
777 **431**, 21–33 (2019).
- 778 9. Terns, M. P. CRISPR-based Technologies: Impact of RNA-targeting Systems. *Mol*  
779 *Cell* **72**, 404–412 (2018).

- 780 10. Makarova, K. S. *et al.* Evolutionary classification of CRISPR-Cas systems: a burst  
781 of class 2 and derived variants. *Nat. Rev. Microbiol.* **18**, 67–83 (2020).
- 782 11. Strecker, J. *et al.* RNA-guided DNA insertion with CRISPR-associated  
783 transposases. *Science* **365**, 48–53 (2019).
- 784 12. Klompe, S. E., Vo, P. L. H., Halpin-Healy, T. S. & Sternberg, S. H. Transposon-  
785 encoded CRISPR-Cas systems direct RNA-guided DNA integration. *Nature* **571**,  
786 219–225 (2019).
- 787 13. Saito, M. *et al.* Dual modes of CRISPR-associated transposon homing. *Cell* **184**,  
788 2441–2453.e18 (2021).
- 789 14. Hou, S. *et al.* CRISPR-Cas systems in multicellular cyanobacteria. *RNA Biol* **16**,  
790 518–529 (2019).
- 791 15. Park, J.-U. *et al.* Structural basis for target site selection in RNA-guided DNA  
792 transposition systems. *Science* **8**, 768–773 (2021).
- 793 16. Chen, W. *et al.* Targeted genetic screening in bacteria with a Cas12k-guided  
794 transposase. *Cell Rep.* **36**, 109635 (2021).
- 795 17. Vo, P. L. H. *et al.* CRISPR RNA-guided integrases for high-efficiency, multiplexed  
796 bacterial genome engineering. *Nat. Biotechnol.* **39**, 480–489 (2021).
- 797 18. Rubin, B. E. *et al.* Species- and site-specific genome editing in complex bacterial  
798 communities. *Nat. Microbiol.* 1–14 (2021).
- 799 19. Reimann, V. *et al.* Specificities and functional coordination between the two Cas6  
800 maturation endonucleases in *Anabaena* sp. PCC 7120 assign orphan CRISPR  
801 arrays to three groups. *RNA Biol.* **17**, 1442–1453 (2020).
- 802 20. Schreiter, E. R. & Drennan, C. L. Ribbon–helix–helix transcription factors:  
803 variations on a theme. *Nat. Rev. Microbiol.* **5**, 710–720 (2007).

- 804 21. Mitschke, J., Vioque, A., Haas, F., Hess, W. R. & Muro-Pastor, A. M. Dynamics of  
805 transcriptional start site selection during nitrogen stress-induced cell differentiation  
806 in *Anabaena* sp. PCC7120. *Proc. Natl. Acad. Sci. USA* **108**, 20130–20135 (2011).
- 807 22. Brenes-Álvarez, M. *et al.* Elements of the heterocyst-specific transcriptome  
808 unravelled by co-expression analysis in *Nostoc* sp. PCC 7120. *Environ. Microbiol.*  
809 **21**, 2544–2558 (2019).
- 810 23. Klucar, L., Stano, M. & Hajduk, M. phiSITE: database of gene regulation in  
811 bacteriophages. *Nucleic Acids Res.* **38**, D366–D370 (2010).
- 812 24. Maxwell, C. S., Jacobsen, T., Marshall, R., Noireaux, V. & Beisel, C. L. A detailed  
813 cell-free transcription-translation-based assay to decipher CRISPR protospacer-  
814 adjacent motifs. *Methods* **143**, 48–57 (2018).
- 815 25. Athukoralage, J. S. *et al.* The dynamic interplay of host and viral enzymes in type  
816 III CRISPR-mediated cyclic nucleotide signalling. *eLife* **9**, e55852 (2020).
- 817 26. Millman, A., Melamed, S., Amitai, G. & Sorek, R. Diversity and classification of  
818 cyclic-oligonucleotide-based anti-phage signalling systems. *Nat. Microbiol.* **5**,  
819 1608–1615 (2020).
- 820 27. Couñago, R. M. *et al.* Structural basis of thiol-based regulation of formaldehyde  
821 detoxification in *H. influenzae* by a MerR regulator with no sensor region. *Nucleic*  
822 *Acids Res.* **44**, 6981–6993 (2016).
- 823 28. Tou, C. J., Orr, B. & Kleinstiver, B. P. Cut-and-Paste DNA Insertion with Engineered  
824 Type V-K CRISPR-associated Transposases. *bioRxiv* 2022.01.07.475005 (2022)  
825 doi:10.1101/2022.01.07.475005.
- 826 29. Brown, N. L., Stoyanov, J. V., Kidd, S. P. & Hobman, J. L. The MerR family of  
827 transcriptional regulators. *FEMS Microbiol. Rev.* **27**, 145–163 (2003).

- 828 30. Julian, D. J., Kershaw, C. J., Brown, N. L. & Hobman, J. L. Transcriptional activation  
829 of MerR family promoters in *Cupriavidus metallidurans* CH34. *Antonie van*  
830 *Leeuwenhoek* 11 (2009).
- 831 31. Godsey, M. H., Zheleznova Heldwein, E. E. & Brennan, R. G. Structural biology of  
832 bacterial multidrug resistance gene regulators. *J. Biol. Chem.* **277**, 40169–40172  
833 (2002).
- 834 32. Ibáñez, M. M., Cerminati, S., Checa, S. K. & Soncini, F. C. Dissecting the metal  
835 selectivity of MerR monovalent metal ion sensors in *Salmonella*. *J. Bacteriol.* **195**,  
836 3084–3092 (2013).
- 837 33. Tardu, M., Bulut, S. & Kavakli, I. H. MerR and ChrR mediate blue light induced  
838 photo-oxidative stress response at the transcriptional level in *Vibrio cholerae*. *Sci.*  
839 *Rep.* **7**, 40817 (2017).
- 840 34. Wang, D. *et al.* Structural analysis of the Hg(II)-regulatory protein Tn501 MerR from  
841 *Pseudomonas aeruginosa*. *Sci. Rep.* **6**, 33391 (2016).
- 842 35. Chang, C.-C., Lin, L.-Y., Zou, X.-W., Huang, C.-C. & Chan, N.-L. Structural basis  
843 of the mercury(II)-mediated conformational switching of the dual-function  
844 transcriptional regulator MerR. *Nucleic Acids Res.* **43**, 7612–7623 (2015).
- 845 36. Jiang, X., Zhang, L., Teng, M. & Li, X. Antibiotic binding releases autoinhibition of  
846 the TipA multidrug-resistance transcriptional regulator. *J. Biol. Chem.* **295**, 17865–  
847 17876 (2020).
- 848 37. Kobayashi, K., Fujikawa, M. & Kozawa, T. Oxidative stress sensing by the iron–  
849 sulfur cluster in the transcription factor, SoxR. *J. Inorg. Biochem.* **133**, 87–91  
850 (2014).
- 851 38. Newberry, K. J. *et al.* Structures of BmrR-drug complexes reveal a rigid multidrug  
852 binding pocket and transcription activation through tyrosine expulsion. *J. Biol.*  
853 *Chem.* **283**, 26795–26804 (2008).

- 854 39. Schumacher, M. A. *et al.* The MerR-like protein BldC binds DNA direct repeats as  
855 cooperative multimers to regulate *Streptomyces* development. *Nat. Commun.* **9**,  
856 1139 (2018).
- 857 40. Santamaría-Gómez, J. *et al.* Role of a cryptic tRNA gene operon in survival under  
858 translational stress. *Nucleic Acids Res.* **49**, 8757–8776 (2021).
- 859 41. Rippka, R., Deruelles, J., Waterbury, J. B., Herdman, M. & Stanier, R. Y. Generic  
860 assignments, strain histories and properties of pure cultures of cyanobacteria.  
861 *Microbiology* **111**, 1–61 (1979).
- 862 42. Elhai, J. & Wolk, C. P. Conjugal transfer of DNA to cyanobacteria. *Meth. Enzymol.*  
863 **167**, 747–754 (1988).
- 864 43. Voß, B. & Hess, W. R. The Identification of Bacterial Non-coding RNAs through  
865 Complementary Approaches. in *Handbook of RNA Biochemistry* 787–800 (John  
866 Wiley & Sons, Ltd, 2014). doi:10.1002/9783527647064.ch34.
- 867 44. Steglich, C. *et al.* The challenge of regulation in a minimal photoautotroph: Non-  
868 coding RNAs in *Prochlorococcus*. *PLOS Gen.* **4**, e1000173 (2008).
- 869 45. Zhu, T., Xie, X., Li, Z., Tan, X. & Lu, X. Enhancing photosynthetic production of  
870 ethylene in genetically engineered *Synechocystis* sp. PCC 6803. *Green Chem.* **17**,  
871 421–434 (2015).
- 872 46. Shin, J. & Noireaux, V. An *E. coli* cell-free expression toolbox: application to  
873 synthetic gene circuits and artificial cells. *ACS Synth. Biol.* **1**, 29–41 (2012).
- 874 47. Wang, Y., Cen, X.-F., Zhao, G.-P. & Wang, J. Characterization of a new GlnR  
875 binding box in the promoter of *amtB* in *Streptomyces coelicolor* inferred a  
876 PhoP/GlnR competitive binding mechanism for transcriptional regulation of *amtB*.  
877 *J. Bacteriol.* **194**, 5237–5244 (2012).

- 878 48. Di Tommaso, P. *et al.* T-Coffee: a web server for the multiple sequence alignment  
879 of protein and RNA sequences using structural information and homology  
880 extension. *Nucleic Acids Res.* **39**, W13–W17 (2011).
- 881 49. Notredame, C., Higgins, D. G. & Heringa, J. T-coffee: a novel method for fast and  
882 accurate multiple sequence alignment *J. Mol. Biol.* **302**, 205–217 (2000).
- 883 50. Suchard, M. A. *et al.* Bayesian phylogenetic and phylodynamic data integration  
884 using BEAST 1.10. *Virus Evol.* **4**, (2018).
- 885 51. Gernhard, T. The conditioned reconstructed process. *J. Theor. Biol.* **253**, 769–778  
886 (2008).
- 887 52. Henikoff, S. & Henikoff, J. G. Amino acid substitution matrices from protein blocks.  
888 *Proc. Natl. Acad. Sci. USA* **89**, 10915–10919 (1992).
- 889 53. Yule, U. A mathematical theory of evolution, based on the conclusions of Dr. JC  
890 Willis, F. R. S. *Phil. Trans. R. Soc.* **213**, 21–87 (1925).
- 891 54. Minor, W., Cymborowski, M., Otwinowski, Z. & Chruszcz, M. HKL-3000: the  
892 integration of data reduction and structure solution--from diffraction images to an  
893 initial model in minutes. *Acta Crystallogr. D Biol. Crystallogr.* **62**, 859–866 (2006).
- 894 55. Yu, F. *et al.* Aqua-rium: an automatic data-processing and experiment information  
895 management system for biological macromolecular crystallography beamlines. *J.*  
896 *Appl. Cryst.* **52**, 472–477 (2019).
- 897 56. McCoy, A. J. *et al.* Phaser crystallographic software. *J. Appl. Crystallogr.* **40**, 658–  
898 674 (2007).
- 899 57. Adams, P. D. *et al.* PHENIX: a comprehensive Python-based system for  
900 macromolecular structure solution. *Acta Crystallogr. D Biol. Crystallogr.* **66**, 213–  
901 221 (2010).
- 902 58. Emsley, P., Lohkamp, B., Scott, W. G. & Cowtan, K. Features and development of  
903 Coot. *Acta Crystallogr. D Biol. Crystallogr.* **66**, 486–501 (2010).

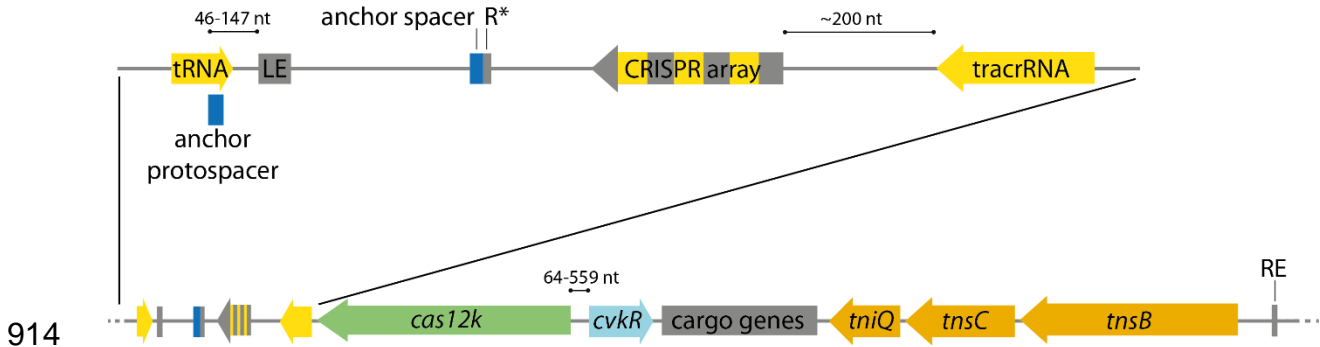


- 904 59. Schrödinger. LLC. *The PyMOL Molecular Graphics System, Version 2.0.* (2015).
- 905 60. Katoh, K. & Standley, D. M. MAFFT Multiple Sequence Alignment Software version  
906 7: improvements in performance and usability. *Mol. Biol. Evol.* **30**, 772–780 (2013).
- 907 61. Okonechnikov, K., Golosova, O., Fursov, M., & UGENE team. Unipro UGENE: a  
908 unified bioinformatics toolkit. *Bioinformatics* **28**, 1166–1167 (2012).
- 909
- 910

911 **Figures**

912

913



914

915

916

917 **Fig. 1. Principal gene arrangement within cyanobacterial CAST systems.** The

918 CAST transposon is displayed from its left end (LE) to its right end (RE). The genes

919 are colored according to function (green: *cas12k*, orange: transposase genes, light

920 blue: CAST regulator gene (*cvkR*), yellow: regions from which non-coding RNA is

921 transcribed, dark gray: cargo genes). On top, the region from the tRNA gene to the

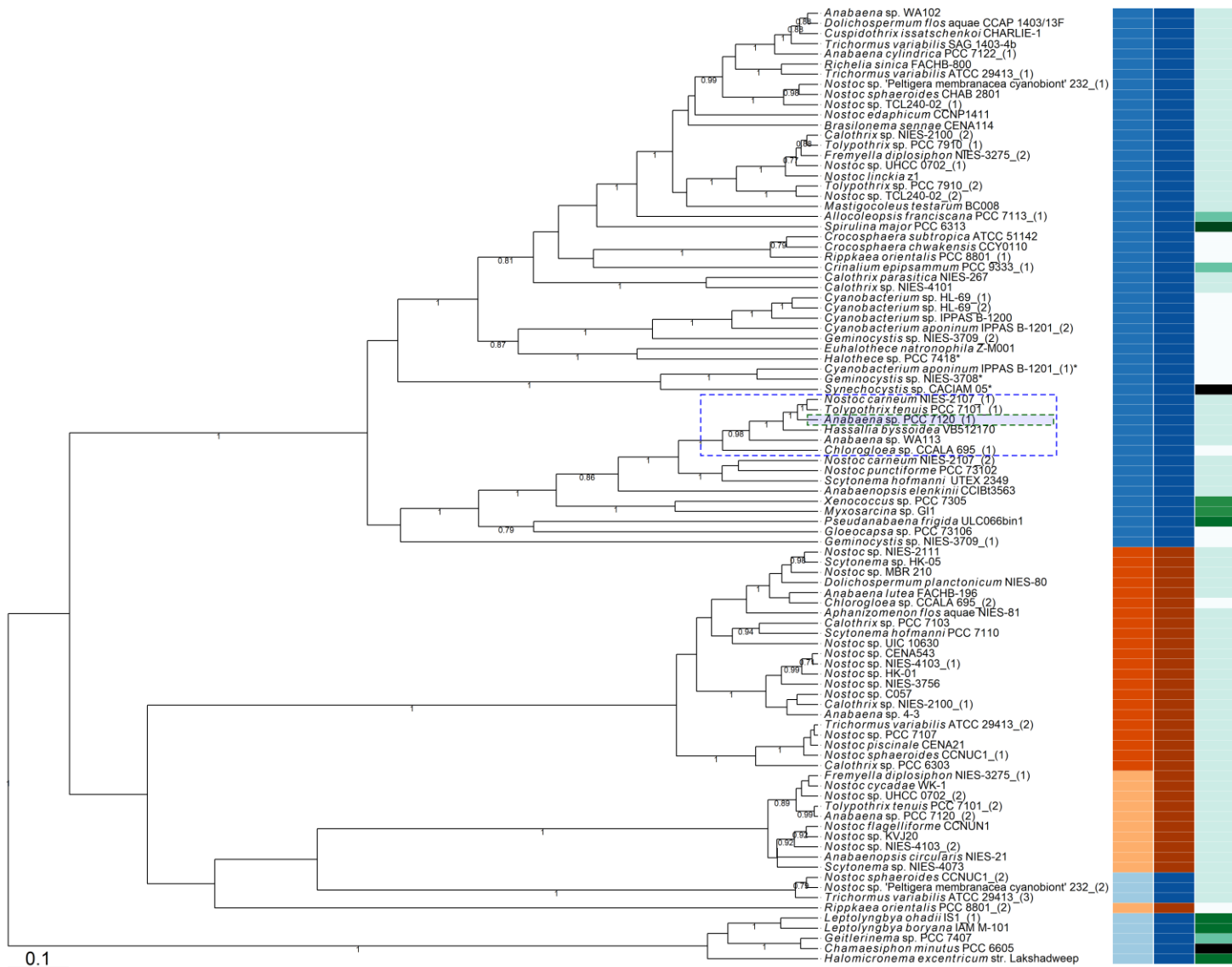
922 tracrRNA is magnified. The CRISPR array is depicted with its repeats (gray) and

923 spacers (yellow) separated from the 17 nt anchor spacer (blue) downstream of the

924 array next to a truncated repeat sequence (R\*; ~12 nt). The scheme is not drawn to

925 scale, but distances of particular interest or mentioned in the text are indicated.

926



**Organism**

- Chroococcales
- Nostocales
- Oscillatoriales
- Pleurocapsales
- Pseudanabaenales
- Spirulinales
- Synechococcales

**Repressor Type**

- CopG
- MerR
- Omega
- unspecific

**DNA-binding Domain**

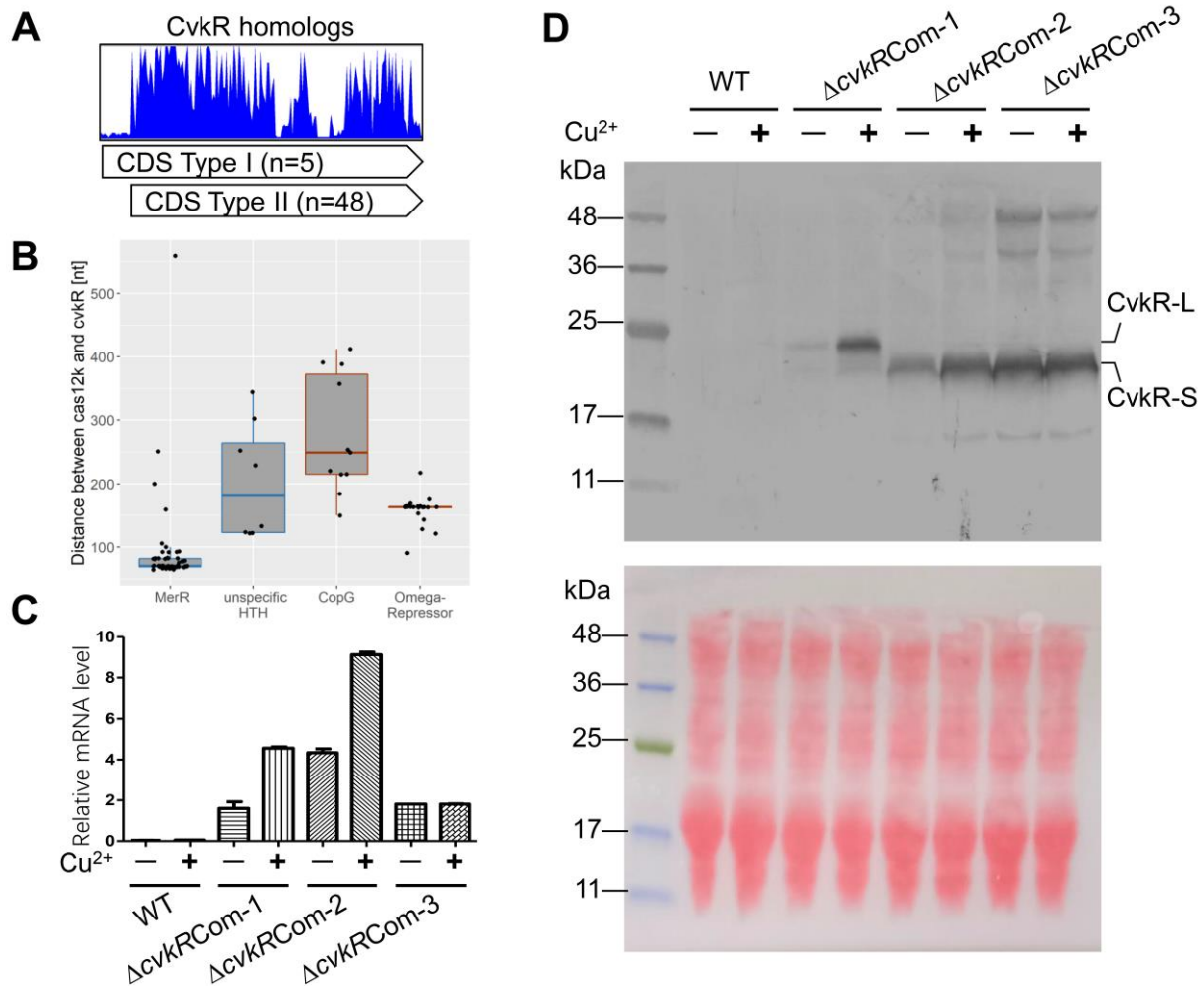
- HTH
- RHH

928

929 **Fig. 2. Phylogenetic tree of all CvkR homologs.** The identified CvkR proteins were aligned using M-coffee<sup>48,49</sup> and analyzed by  
930 BEAST<sup>50</sup>. As a prior tree module, we used a Yule process for 1,000,000 states, log processed every 1,000 steps. The resulting tree is  
931 depicted with branches labeled with their respective posterior probability until a threshold of 0.5. For better recognition, the proteins were  
932 also labeled with their host organism as well as their repressor type and DNA interaction domain. The *Anabaena* 7120 CvkR (Alr3614)  
933 (NCBI: BAB75313.1) (green dashed box) is marked as well as its most similar homologs (>70% shared identity, highlighted by a blue-  
934 dashed box). Asterisks label four instances of CvkRs fused to an *hsdR* restriction enzyme domain. The multiple sequence alignment is  
935 available as **supplemental dataset S1**.

936

937



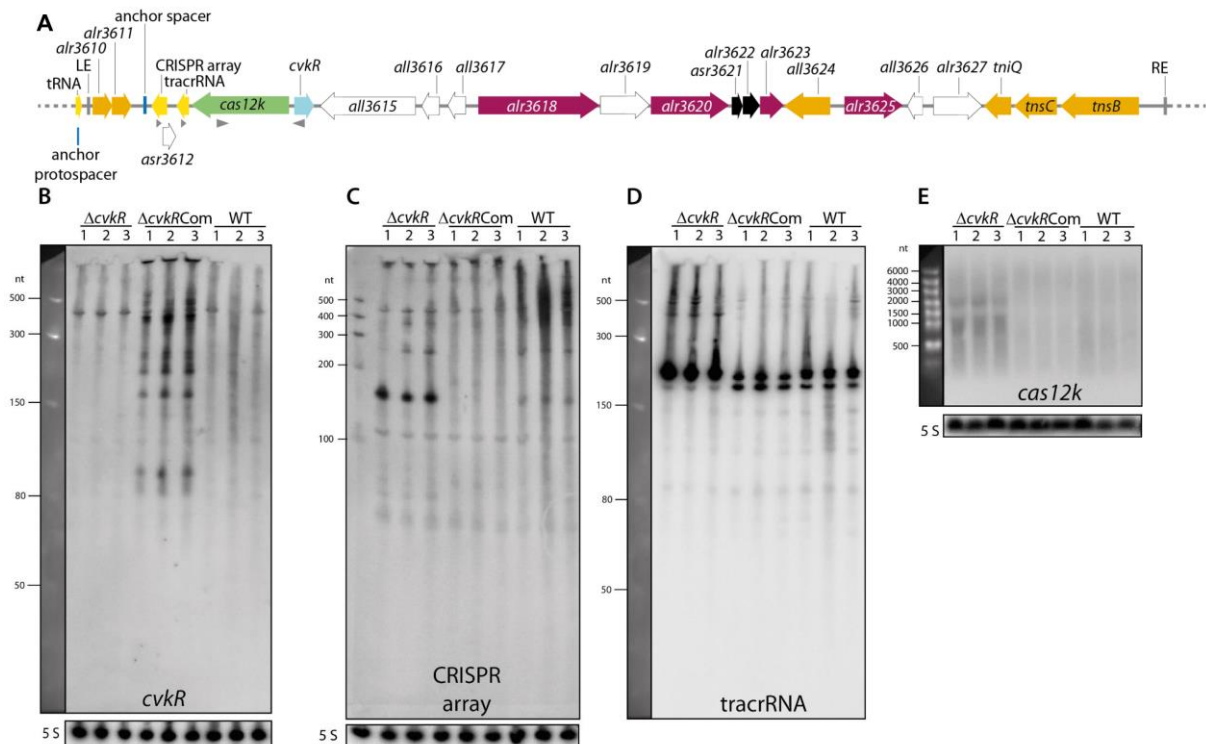
938

939

940 **Fig. 3. Leaderless expression of *cvkR* genes.** **A.** Deduced amino acid sequence  
 941 alignment of 53 MerR-family CvkR homologs. The sequences of the MerR-family CvkR  
 942 homologs for the multiple sequence alignment were recovered from public databases  
 943 and are available as **supplemental dataset S2**. The sequences were aligned using  
 944 MAFFT<sup>60</sup> and visualized with UGENE<sup>61</sup>. Only the N-terminal ~200 amino acids are  
 945 displayed for clarity reasons. **B.** Distances between the *cas12k* effector complex and  
 946 *cvkR* genes are plotted according to the respective type of regulator, MerR-like (53  
 947 instances), CopG-like (11 cases), Omega-like (22 cases) and nonspecific HTH  
 948 domain-containing proteins (8 cases). The box plots are colored according to the  
 949 respective DNA-binding domain (HTH: blue; RHH: red). **C.** qRT-PCR analyses verify

950 that *cvkR* is transcribed in  $\Delta cvkR$ Com strains. The amounts of *cvkR* transcripts were  
951 normalized to those of *rnpB* as an internal standard. Three independent experiments  
952 were performed, which showed consistent results. **D.** Western blot analyses confirmed  
953 the leaderless expression of CvkR. Upper panel, Western blot against the C-terminal  
954 3xFLAG tag; Lower panel, ponceau S staining shows that equal amounts of protein  
955 were loaded (100  $\mu$ g). The calculated molecular masses for CvkR-S and CvkR-L were  
956 20.03 kDa and 22.41 kDa, respectively. Two independent experiments were  
957 performed, which showed consistent results. The  $\Delta cvkR$ Com-1, 2 and 3 strains are  
958 detailed in **Fig. S1C**.

959



960

961

962 **Fig. 4. The CRISPR-associated transposase system in *Anabaena* 7120 (AnCAST)**

963 **and the effects of *cvkR* deletion and overexpression on transcript accumulation.**

964 **A.** Gene arrangement within the 24,963 nt element of *Anabaena* 7120 encompassing

965 the *cvkR* gene encoding a transcriptional regulator relative to the effector, cargo and

966 Tn7 genes. The location of probes used for hybridizations in panels B to C is indicated

967 by gray triangles. Gene functions are color-coded as in **Fig. 1**. In addition, we used

968 pink to highlight RM genes and black to indicate a toxin-antitoxin module. **B.** Northern

969 hybridization against *cvkR* mRNA. A signal of ~450 nt is due to cross-hybridization, as

970 also occurred in  $\Delta cvkR$ . The RiboRuler Low Range RNA Ladder (Thermo Fisher

971 Scientific) was used as a size marker. **C.** Northern hybridization against the CRISPR

972 array (S3-S4). **D.** Northern hybridization against tracrRNA. The expected length of the

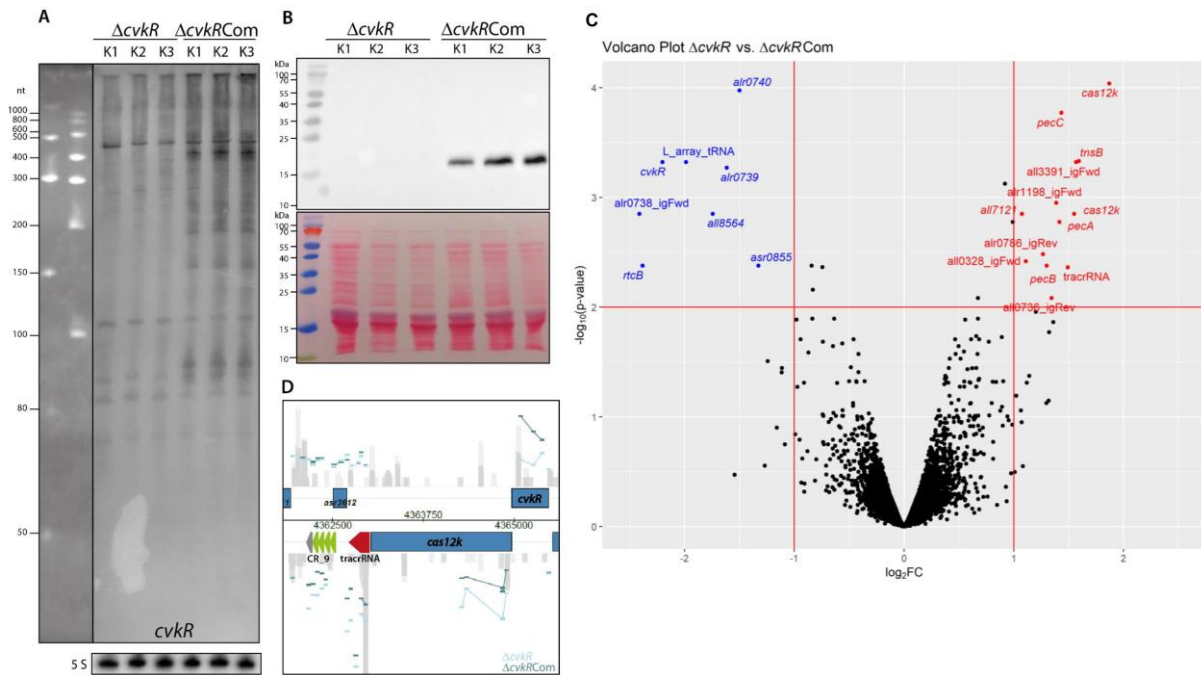
973 tracrRNA according to transcriptome data (accession number PRJNA624132 in

974 NCBI's short reads archive<sup>19</sup>) is approximately 210 nt. The Low Range ssRNA Ladder

975 (NEB) was used as a size marker. **E.** Northern hybridization against *cas12k*. The



976 expected length of the *cas12k* mRNA is not known, as the transcript level was below  
977 the detection limit in WT. The gene length is 1.92 kb. RiboRuler High Range RNA  
978 Ladder (Thermo Fisher Scientific) was used as a size marker. All gels and membranes  
979 were checked for equal loading by staining with ethidium bromide and hybridization to  
980 the 5S rRNA (except in panel D because the same membrane was rehybridized as in  
981 panel B). Twenty micrograms of total RNA of the WT, the deletion mutant  $\Delta cvkR$  and  
982 the complementation mutant  $\Delta cvkRCom$  were separated on 10% PAA 8.3 M urea  
983 (panels B to D) or 1.5% formaldehyde-agarose gels.  
984



985

986

987 **Fig. 5. Microarray analysis of the *cvkR* deletion and complementation mutants.**

988 **A.** Northern blot hybridization against *cvkR*. The expected length of the *cvkR* mRNA is  
 989 unknown because the transcript level in WT is below the detection limit. The gene  
 990 length is 453 bp. Total RNA (20  $\mu$ g) was loaded on a 10% PAA 8.3 M urea gel. The  
 991 Low Range ssRNA Ladder (NEB) and the RiboRuler Low Range RNA Ladder (Thermo  
 992 Fisher Scientific) were used as size markers. **B.** Western blot against CvkR with an N-  
 993 terminal 3xFLAG tag (upper panel); the stained membrane is shown in the lower panel.  
 994 The calculated molecular mass for CvkR is 20.16 kDa. The prestained PageRuler  
 995 (Thermo Fisher Scientific) was used as a size marker. Ten micrograms of total protein  
 996 were loaded on a 15% SDS-PAGE gel. **C.** Volcano plot of  $\Delta cvkR$  and  $\Delta cvkRCom$   
 997 transcriptome analyses. The horizontal line marks the p value cutoff of 0.01, while the  
 998 two vertical lines mark the fold change cutoff of  $|\log_2| \geq 1$ . The features above these  
 999 thresholds showed significant downregulation (8 transcripts, blue) or upregulation (13  
 1000 transcripts, red). **D.** Visualization of the most differentially expressed region in the  
 1001 *Anabaena* 7120 genome, which belongs to the AnCAST system. Positions of the

1002 tracrRNA and the CRISPR array are annotated; individual probes are indicated by  
1003 short horizontal bars and colored in light blue for the deletion mutant  $\Delta cvkR$  and in dark  
1004 blue for the complementation mutant  $\Delta cvkRCom$ .  
1005

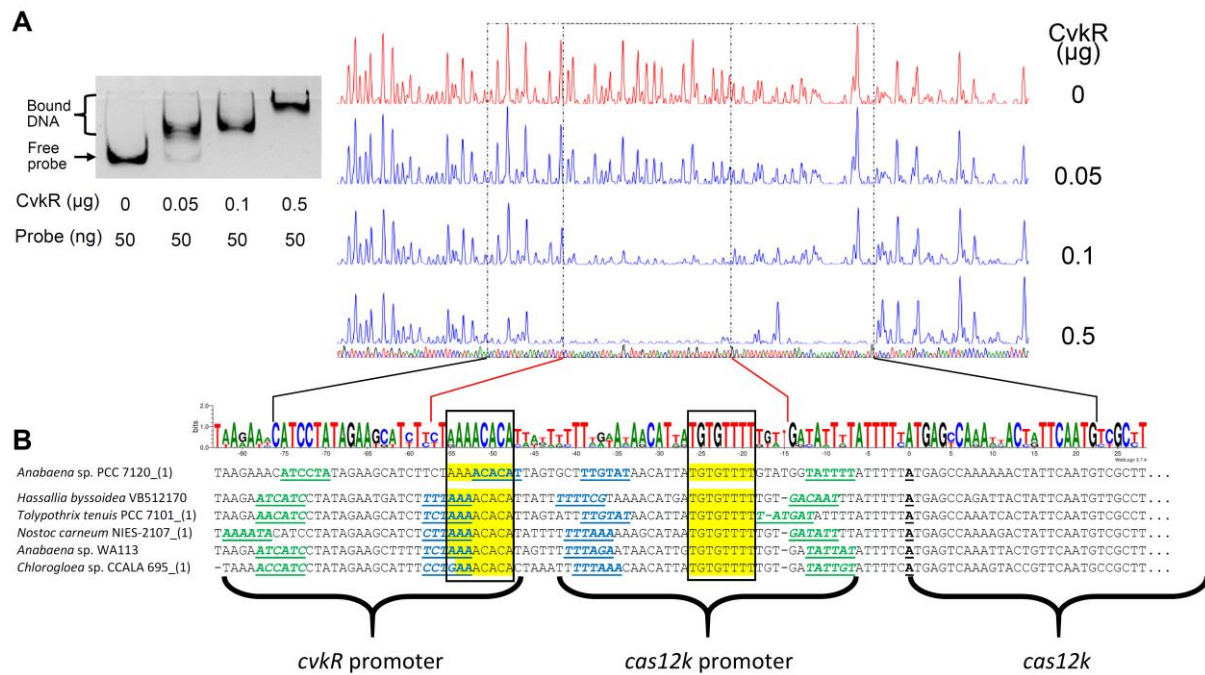


**Fig. 6. CvkR interaction with *cas12k* promoter fragments and predicted binding**

**motifs. A.** Left panel, EMSA showing the direct binding of different amounts of CvkR

to the *cas12k* promoter DNA. Right panel, DNase I footprinting assay. The *cas12k*

promoter DNA was digested in the presence of different concentrations of CvkR. The

fragmentation pattern indicated a core region of 43 nt that was protected from DNase

I degradation in the presence of CvkR (inner dot-and-dashed lines) embedded in a

longer segment protected at higher CvkR concentrations (outer dot-and-dashed lines).

**B.** The intergenic spacers between *cvkR* and *cas12k* from 6 different CASTs were

aligned and analyzed for potential promoter elements. The -35 (blue) and -10 (green)

regions for both promoters as well as the transcription start site of *cas12k* (black) are

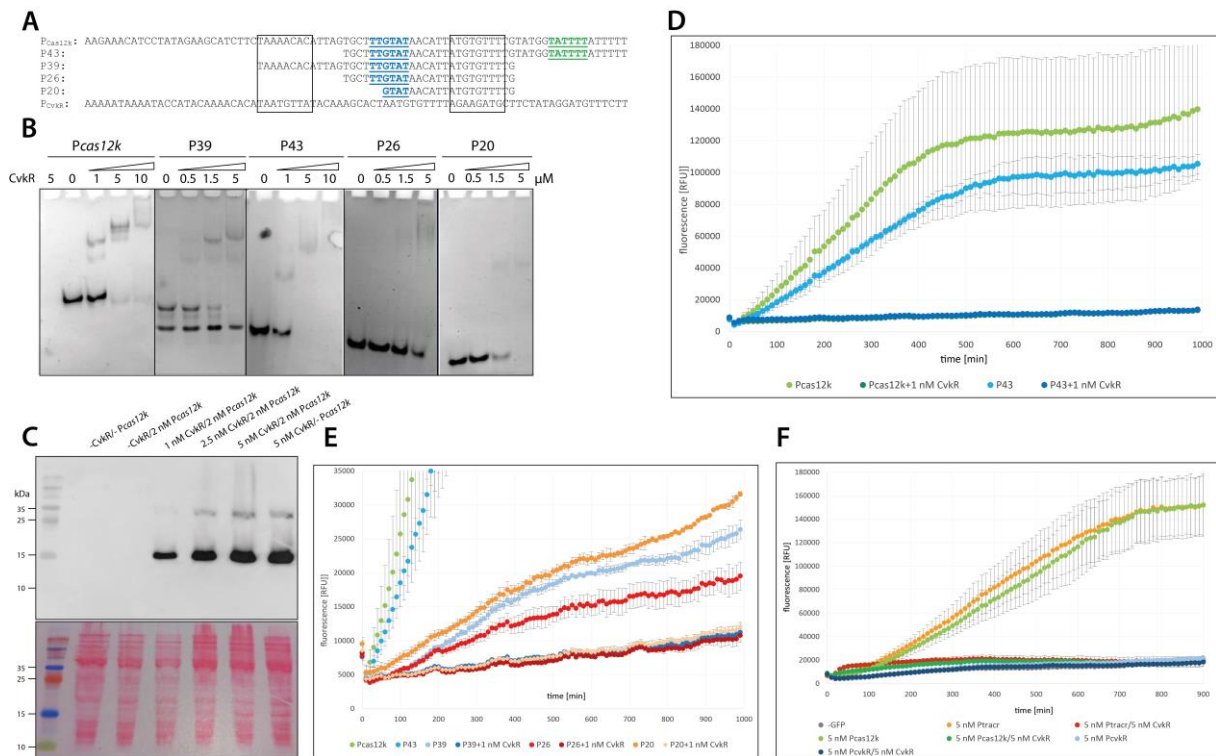
marked, which were previously identified<sup>21</sup> or predicted by PromoterHunter<sup>23</sup>

(nucleotides in italics). The CvkR protected region in the DNase I footprinting assay is

marked, which contains a conserved inverted repeat surrounding the -35 region of the

*cas12k* promoter (boxed and highlighted in yellow). The sequences are also visualized

as sequence logo.



1023

1024

1025 **Fig. 7. Assays to test *cas12k* promoter elements.** **A.** Sequences of the tested

1026 promoter fragments. Putative -35 and -10 *cas12k* promoter elements are shown in blue

1027 and green, respectively. **B.** EMSA of the  $P_{cas12k}$  full-length and truncated fragments

1028 after DNA incubation for 40 min with different concentrations of CvkR. **C.** CvkR was

1029 expressed from vector pET28a and was detected by Western blot analysis via the N-

1030 terminal 6xHis tag (upper panel), and the stained membrane is shown in the lower

1031 panel. The corresponding size for 6xHis-CvkR is 19.9 kDa. The prestained PageRuler

1032 (Thermo Scientific) was used as a size marker. **D.** The full-length version of  $P_{cas12k}$  and

1033 the P43 fragment encompassing 43 nt upstream of the *cas12k* TSS were tested in the

1034 TXTL system<sup>24</sup> for their capacity to drive deGFP expression and mediate repression

1035 upon parallel expression of CvkR. CvkR was expressed together with the

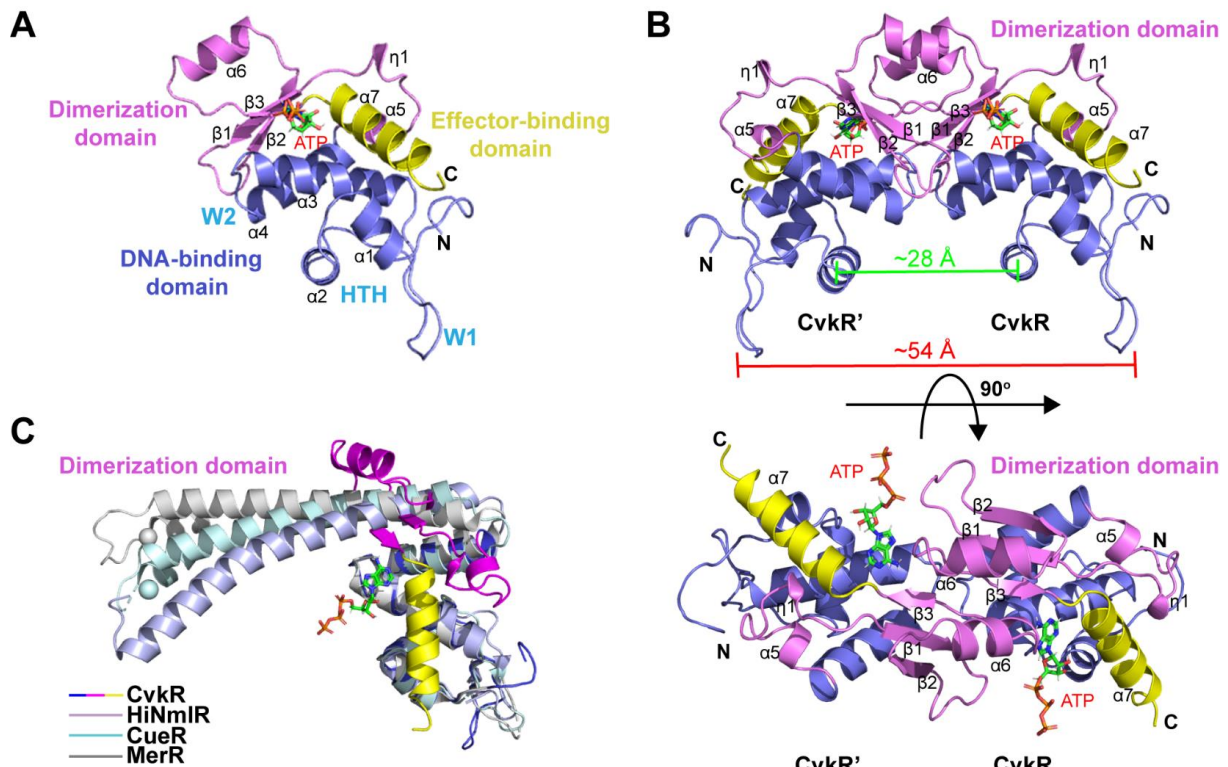
1036 corresponding p70a plasmids (5 nM) with the two promoter variants upstream of

1037 deGFP. **E.** TXTL assay for the promoter sequences P39 (positions -56 to -18 relative

1038 to the TSS of *cas12k*), P26 (positions -42 to -18) and P20 (positions -42 to -18). **F.**

1039 TXTL assay to compare the promoter activities of *cas12k*, *cvkR* and *tracrRNA* ( $P_{cas12k}$ ,  
1040  $P_{cvkR}$ ,  $P_{tracr}$ ). CvkR was used to repress transcription. Error bars show standard  
1041 deviations calculated from 2 technical replicates in panels D to F.  
1042



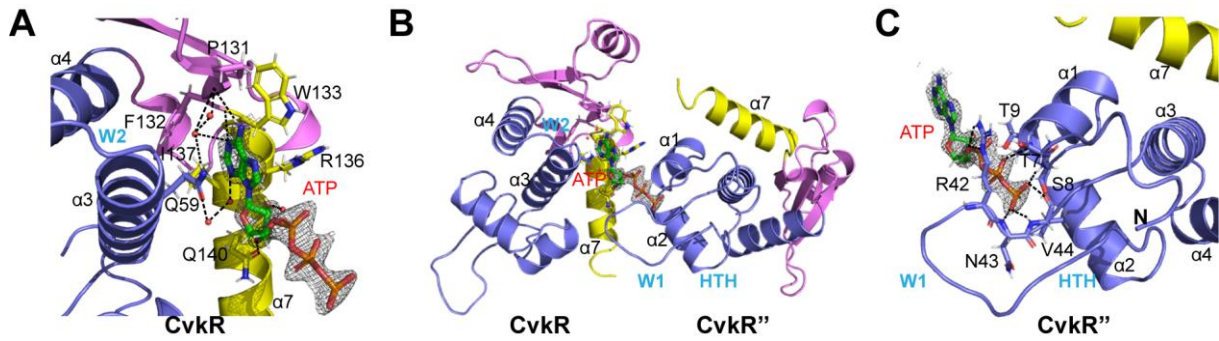


1043

1044

1045 **Fig. 8. Overall structure of CvkR.** **A.** Ribbon representation of the CvkR-ATP  
1046 complex in ASU. The DNA-binding, dimerization, and effector-binding domains are  
1047 shown in blue, magenta, and yellow, respectively. The typical helix-turn-helix (HTH)  
1048 and two “wing” loops W1 and W2 in the DNA-binding domain are indicated. The ATP  
1049 ligand is represented in green sticks and colored by the atom type. The secondary  
1050 structure elements of CvkR are labeled. **B.** Ribbon representation of the homodimer  
1051 structure of CvkR through a crystallographic symmetry operator. The novel  
1052 dimerization is formed by three antiparallel  $\beta$ -strands ( $\beta 2$ - $\beta 1$ - $\beta 3$ ) and one short  $\alpha$ -helix  
1053 ( $\alpha 6$ ) from the two protomers in the dimer. The distances between two  $\alpha 2$ -helices and  
1054 between two W1 regions are measured and labeled, respectively. **C.** Structural  
1055 comparison of MerR-type proteins. The DNA-binding domain of one subunit of CueR  
1056 (PDB code 1Q07), MerR (PDB code 4UA1) and HiNmIR (PDB code 5D90) is  
1057 separately superimposed on that of CvkR. The structural data can be accessed under  
1058 the PDB accession number 7XN2.



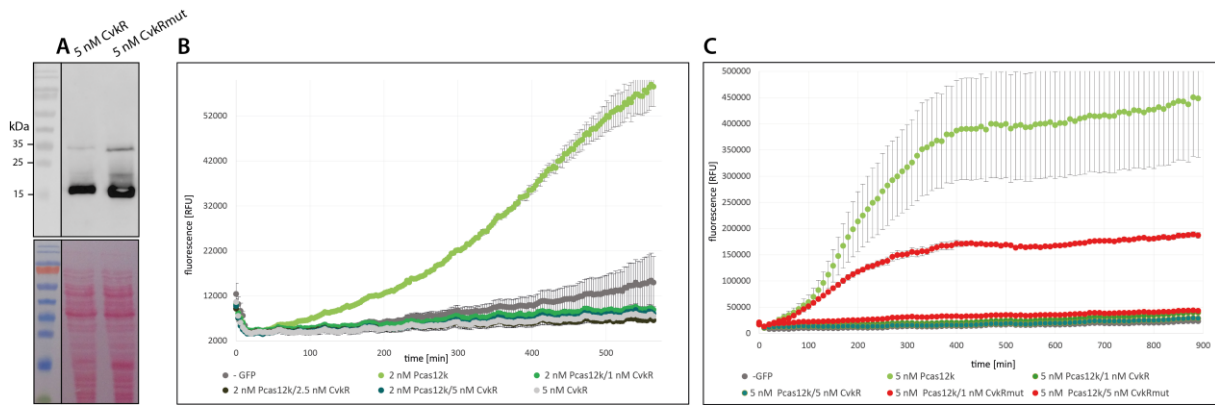


1059

1060

1061 **Fig. 9. ATP binding site of CvkR.** **A.** Close view of the ATP-binding site in the CvkR  
1062 monomer. **B.** Overview of the ATP-binding site between two CvkR molecules (CvkR  
1063 and CvkR''). **C.** Close view of the ATP triphosphate group-binding site in CvkR''. The  
1064 ATP ligand is represented as green sticks and colored by the atom type. The 2Fo-Fc  
1065 density for ATP is contoured in blue at 1.5  $\sigma$ . The key residues involved in ATP binding  
1066 are shown as sticks and labeled with black. The hydrogen bonds are shown by the  
1067 dashed lines. The water molecules involved in hydrogen bonds are presented as red  
1068 spheres.

1069



1070

1071

1072 **Fig. 10. TXTL assay with CvkR and CvkRmut and different promoters. A.** To

1073 address the relevance of possibly critical residues according the CvkR crystal structure

1074 (**Fig. 8 and 9**), six amino acids were substituted by Ala (R19A-R20A-Q23A-K40A-

1075 R42A-N66A), yielding protein CvkRmut. *Anabaena* 7120 CvkR and CvkRmut were

1076 expressed in the TXTL system<sup>24</sup> from pET28a and detected by Western blot analysis

1077 via their N-terminal 6xHis tag (upper panel). The stained membrane is shown below.

1078 The corresponding molecular masses are 19.9 kDa for 6xHis-CvkR and 19.5 kDa for

1079 6xHis-CvkRmut. **B.** The promoter of *cas12k* ( $P_{cas12k}$ ) was used to express deGFP from

1080 plasmid p70a (2 nM) in the absence or presence of different amounts of plasmid

1081 pET28a expressing CvkR. Error bars show the standard deviation and are derived from

1082 two technical replicates. **C.** TXTL assay to test the regulatory capacity of CvkRmut

1083 compared to CvkR for repressing deGFP fluorescence expressed from p70a under the

1084 control of  $P_{cas12k}$  (5 nM). Error bars show the standard deviation and are derived from

1085 2 technical replicates. All experiments were repeated twice independently. The TXTL

1086 reactions were performed at 29 °C overnight, and fluorescence was measured every

1087 10 min in a Wallac 1420 Victor 2 microplate reader.